Molecular Cell
Article

Dynamics of Histone H3 Deposition In Vivo Reveal a Nucleosome Gap-Filling Mechanism for H3.3 to Maintain Chromatin Integrity

Dominique Ray-Gallet,[1,2] Adam Woolfe,[1,2,7] Isabelle Vassias,[1,2,7] Céline Pellentz,[1,2,6] Nicolas Lacoste,[1,2] Aastha Puri,[3] David C. Schultz,[3] Nikolay A. Pchelintsev,[4] Peter D. Adams,[4] Lars E.T. Jansen,[5] and Geneviève Almouzni[1,2,*]
[1]Centre de Recherche, Institut Curie, 75248 Paris, France
[2]Centre National de la Recherche Scientifique, Unité Mixte de Recherche 218, 75248 Paris, France
[3]Protein Production, Libraries and Molecular Screening Facility, The Wistar Institute, Philadelphia, PA 19104, USA
[4]Epigenetics of Cancer and Ageing, The Beatson Institute for Cancer Research, Garscube Estate, Switchback Road, Bearsden, Glasgow G61 1BD, UK
[5]Instituto Gulbenkian de Ciência, Rua da Quinta Grande 6, 2780-156 Oeiras, Portugal
[6]Present address: Laboratoire du Métabolisme de l'ADN et Réponses aux Génotoxiques, SBIGeM, iBiTecS, CEA, 91191 Gif-sur-Yvette, France
[7]These authors contributed equally to this work
*Correspondence: almouzni@curie.fr
DOI 10.1016/j.molcel.2011.12.006

SUMMARY

Establishment of a proper chromatin landscape is central to genome function. Here, we explain H3 variant distribution by specific targeting and dynamics of deposition involving the CAF-1 and HIRA histone chaperones. Impairing replicative H3.1 incorporation via CAF-1 enables an alternative H3.3 deposition at replication sites via HIRA. Conversely, the H3.3 incorporation throughout the cell cycle via HIRA cannot be replaced by H3.1. ChIP-seq analyses reveal correlation between HIRA-dependent H3.3 accumulation and RNA pol II at transcription sites and specific regulatory elements, further supported by their biochemical association. The HIRA complex shows unique DNA binding properties, and depletion of HIRA increases DNA sensitivity to nucleases. We propose that protective nucleosome gap filling of naked DNA by HIRA leads to a broad distribution of H3.3, and HIRA association with Pol II ensures local H3.3 enrichment at specific sites. We discuss the importance of this H3.3 deposition as a salvage pathway to maintain chromatin integrity.

INTRODUCTION

Distinct histone variants mark specific chromatin states (Kouzarides, 2007; Talbert and Henikoff, 2010); however, the mechanisms used to achieve this defined distribution remain unclear. In mammals, several histone H3 variants have been identified among which the replicative and replacement variants—H3.1 and H3.3, respectively—show only a 5 amino acid difference (Szenker et al., 2011). The increased expression of replicative histones during S phase ensures the major source of histones during replication (Corpet and Almouzni, 2009; Groth et al., 2007; Kaufman and Rando, 2010). In contrast, the constitutive expression of the replacement H3.3 variant throughout the cell cycle and in quiescence provides a continuous source in all instances (Wu et al., 1982). While H3.3 is highly enriched within actively transcribed genes (Jin et al., 2009; Mito et al., 2005; Wirbelauer et al., 2005), its use during sperm reprogramming (Loppin et al., 2005; Torres-Padilla et al., 2006; van der Heijden et al., 2005) and its accumulation at telomeric (Goldberg et al., 2010; Wong et al., 2009) and pericentric heterochromatin (Drané et al., 2010) suggest various means for H3.3 deposition independent of transcription.

Histone chaperones are currently considered the most likely candidates responsible for specific histone variant deposition (De Koning et al., 2007; Ray-Gallet and Almouzni, 2010). The respective presence of chromatin assembly factor-1 (CAF-1) with H3.1 and the histone regulator A (HIRA) complex with H3.3 in soluble complexes have implicated these histone chaperones in the specific deposition of these variants (Tagami et al., 2004). CAF-1 consists of three subunits p150, p60, and p48 and promotes histone deposition during replication and UV-damage repair (Gaillard et al., 1996; Polo et al., 2006; Smith and Stillman, 1989). In contrast to CAF-1, HIRA promotes histone deposition independently of DNA synthesis as shown in *X. laevis* egg extracts (Ray-Gallet et al., 2002). Recent data show that HIRA is in a complex that also contains calcineurin-binding protein 1 (Cabin1) and ubinuclein 1 (UBN1) (Balaji et al., 2009; Banumathy et al., 2009; Elsaesser and Allis, 2010; Rai et al., 2011). Notably, these three components have counterparts in yeast that constitute the HIR complex (Amin et al., 2011). More recently, the report of other separate H3.3 chaperones, namely DEK (Sawatsubashi et al., 2010) and a complex comprised of the death-associated protein (DAXX) and the alpha-thalassemia/mental retardation X-linked syndrome protein (ATRX) (Drané et al., 2010; Goldberg et al., 2010; Lewis et al., 2010; Wong et al., 2010) have raised the possibility that, beside the HIRA-dependent process, additional pathways could contribute to distinct H3.3 local

enrichment. The recurrent observation that histone chaperones regulation is affected in cancer, with CAF-1 and Asf1b marking aggressive breast tumors (Corpet et al., 2011; Polo and Almouzni, 2005; Polo et al., 2010), DEK rearrangement in acute myeloid leukemia (von Lindern et al., 1992), and mutation in DAXX/ATRX in pancreatic neuroendocrine tumors (Jiao et al., 2011) underline the importance of understanding how their handling of histones possibly relate to tumorigenesis.

Recent advances using chromatin immunoprecipitation combined with high-throughput analysis with microarrays or deep sequencing (ChIP-seq) have enabled a global view of histone variant dynamics and enrichment at particular genomic regions. Combination of these analyses with knockout experiments in mouse embryonic stem cells (ESCs), recently revealed that HIRA has a critical role for H3.3 accumulation at promoters, active genes, and particular regulatory elements, distinct from DAXX/ATRX which has been implicated in H3.3 enrichment at telomeres (Goldberg et al., 2010). While an enrichment profile reflects the accumulation of a histone variant in a steady state at an endpoint, it is important to realize that this enrichment is the result of the combined events of deposition, eviction, and maintenance. Thus, to fully define which of these events can be affected by a particular factor, it is necessary to develop an appropriate technology in which a distinction between new and old histones can be made. In this respect, a new method termed CATCH-IT (covalent attachment of tags to capture histones and identify turnover) enabled the measurement of incorporation and turnover rates of newly synthesized histones genome-wide in *Drosophila* cells (Deal et al., 2010). However, this technique provides only an average picture across a cell population, rather than on a cell-by-cell basis, and does not distinguish between histone variants. A unique and alternative strategy employs the SNAP-tag, a small self-labeling enzyme that can be fluorescently pulse labeled in vivo. Here, we apply SNAP-tag technology for visualization of specific newly synthesized tagged histones on a cell-by-cell basis (Keppler et al., 2003). Indeed, this approach has proven powerful in following the inheritance and deposition of the specific H3 variant CENP-A during late mitosis (Dunleavy et al., 2011; Foltz et al., 2009; Jansen et al., 2007).

Using the SNAP-tag technology combined with genome wide analysis, we study in vivo deposition of H3.1 and H3.3 histone variants. By exploiting this approach, both qualitatively on a cell-by-cell basis and quantitatively on a population of cells, we provide a view concerning how CAF-1- and HIRA-mediated deposition pathways can be interrelated and how the HIRA complex can be targeted for H3.3 incorporation. Based on these data, we discuss how the HIRA-dependent H3.3 deposition can act as a salvage pathway to maintain chromatin integrity at any place where nucleosomal organization is compromised and how this impacts on genome function.

RESULTS

An In Vivo Visualization Assay for Newly Synthesized H3.1 and H3.3 Deposition

To monitor newly synthesized histone deposition in vivo, we used two HeLa cell lines stably expressing respectively H3.1 or H3.3 tagged with three HA epitopes and SNAP. The SNAP polypeptide reacts covalently in vivo with cell-permeable fluorescent or nonfluorescent substrates and enables specific visualization of newly synthesized histones (Jansen et al., 2007) (see Figure S1 available online). We first validated in both cell lines the efficiency of our in vivo deposition assay based on "quench-chase-pulse" labeling. Microscopy analysis (Figure 1A) shows that the "pulse" labeled both preexisting H3.1 and H3.3 effectively, while the "quench-pulse" gives only background confirming the efficiency of quenching. The "quench-chase-pulse" shows a reduced TMR-Star staining consistent with the short pulse labeling of newly synthesized histones when compared to the one corresponding to all preexisting tagged histones. Part of the newly synthesized histones is not solubilized by detergent extraction reflecting their incorporation into chromatin. To quantify the distinct histone populations, using extracts from the same cells, we resolved proteins by gel electrophoresis and analyzed the fluorescently pulse-labeled bands corresponding to the different forms of H3.1 and H3.3 (Figure 1B). We found a comparable value for the proportion of total newly synthesized tagged histones H3.1 and H3.3 (the ratio of new total histones H3.1/H3.3 is 0.88) as expected for an ectopically driven expression for both tagged histones throughout the cell cycle. However, the ratio of new incorporated histones H3.1/H3.3 is 0.53 reflecting the more limited incorporation of H3.1 restricted to replicating cells, whereas deposition of H3.3 occurs throughout the cell cycle (see below). It is interesting to note though that if one would consider that the efficiency of deposition was perfectly equal for both variants, then this number should be even lower given that S phase represents about 40% of total cells. This indicates that, while restricted to S phase, H3.1 deposition involves a potent deposition mechanism.

We conclude that cell lines expressing SNAP-tagged histones are a powerful tool to analyze in vivo the mechanisms of de novo deposition of newly synthesized H3.1 or H3.3 both at an individual cell level and in a quantitative manner using the "quench-chase-pulse" assay.

Newly Deposited H3.1 Overlaps with the Replication Sites In Vivo, Whereas H3.3 Does Not

To further analyze incorporation of H3.1 and H3.3 in vivo during S phase, we exploited the "quench-chase-pulse" validated strategy combined with the use of a deoxyribonucleotide precursor EdU (5-ethynyl-2′-deoxyuridine) to detect replicating cells. The addition of EdU at the time of the "pulse" enables one to compare incorporation of newly synthesized histones with the replication sites (Figure 2A). The replicating cells (EdU positive) showed a strong labeling with newly incorporated H3.1 whereas in the nonreplicating cells (EdU negative) almost no labeling occurred (Figure 2B). In contrast, in both replicating and nonreplicating cells, newly synthesized H3.3 got incorporated (Figure 2B). Newly incorporated H3.1 strictly colocalized with the replication sites, and this was most obvious in mid or late S phase (Figure 2C). In contrast, although incorporation of newly synthesized H3.3 occurred in replicating cells, the labeling pattern did not overlap with replication sites, as best observed in mid and late S phase (Figure 2C), raising the interesting possibility that an efficient H3.1 deposition may prevent H3.3

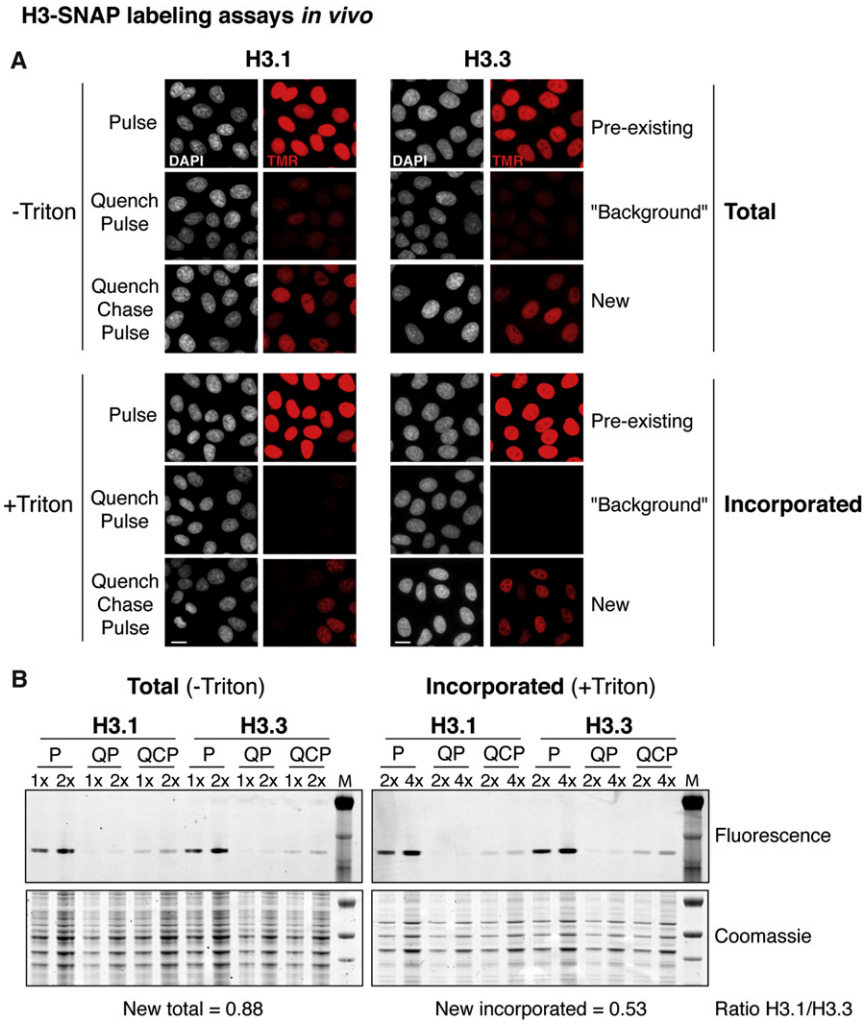

Figure 1. An In Vivo Visualization Assay for Newly Synthesized H3.1 and H3.3 Deposition

(A) Fluorescent microscopy visualization of H3.1- and H3.3-SNAP after in vivo labeling assays with red fluorescent TMR-Star in pulse, quench-pulse, and quench-chase-pulse experiments. The pulse labels pre-existing H3-SNAP, the quench-pulse quenches pre-existing H3-SNAP with nonfluorescent block preventing their subsequent labeling with TMR-Star (background), and the quench-chase-pulse labels new H3-SNAP synthesized during the 2 hr-chase (see Figure S1). Either total (–triton) or incorporated (+triton) H3.1-SNAP and H3.3-SNAP are visualized. Scale bars represent 10 μm.

(B) Gel analysis of total (–triton) or incorporated (+triton) H3.1-SNAP and H3.3-SNAP after in vivo labeling assays in pulse (P), quench-pulse (QP), and quench-chase-pulse (QCP) experiments. Extracts from labeled cells (–triton or +triton) were used for NuPAGE gel electrophoresis. The fluorescent bands corresponding to the labeled H3.1- and H3.3-SNAP were visualized and quantified after normalization to Coomassie staining. We calculated the ratios of H3.1/H3.3 for new total and new incorporated labeled histones, respectively. The indicated ratios correspond to the average value derived from four experiments. Standard deviations for the total new H3.1/H3.3 ratio is 0.08 and for newly incorporated 0.03 (n = 4).

See also Figure S1.

incorporation. Furthermore, when inhibiting DNA synthesis using aphidicolin, the labeling of newly incorporated H3.1 dramatically decreased when compared with H3.3 (Figure S2).

We conclude that the de novo deposition of H3.1 occurs mainly during S phase colocalizing with replication sites, whereas H3.3 de novo deposition occurs throughout interphase including S phase without overlapping with replication sites.

Alternative Deposition of H3.3 at Replication Sites When H3.1 Incorporation Is Impaired by CAF-1 Depletion

We next exploited our in vivo deposition assay to directly assess the role of histone chaperones in the deposition step. We transfected cells expressing either H3.1 or H3.3 with small interfering RNA (siRNA) against the p60 subunit of the H3.1 chaperone CAF-1 prior to the "quench-chase-pulse" and the labeling of replication sites with EdU (scheme Figure 3A). We checked cell cycle profiles by flow cytometry analysis and verified CAF-1 p60 downregulation by western blot analysis (Figure S3A). Newly synthesized H3.1 labeling decreased in cells depleted from p60, yet replicating as attested by the EdU staining (Figure 3B). To quantify these data, instead of gel analysis as in Figure 1B, which only give a global estimation and cannot permit to selectively analyze replicating cells, we choose a microscopic method using image acquisitions. Notably, this type of quantification allows us to specifically focus on replicating cells (EdU positive) and has proven more accurate than the global gel fluorescence analysis (see the Experimental Procedures). We estimated about 50% reduction by quantification of TMR fluorescence intensity for H3.1 and only 10% for H3.3 in p60-depleted cells (Figure 3B). Comparison of cytosolic, nuclear and chromatin fractions further supported these results (Figure S3D).

Remarkably, with a closer inspection, when focusing on replication foci, with two sets of siRNA against p60 we could detect H3.3 incorporation overlapping the replication sites marked by EdU, a pattern not detected in sicont-cells (Figure 3B and Figure S3C). When selecting EdU-positive cells and examining the replication foci, we found that the single depletion of p60 enabled us to detect 20% of replicating cells that exhibited an overlap between H3.3 incorporation signal, detected with TMR, and EdU (Figure 3C). To identify which key chaperone promotes this unusual H3.3 deposition at replication sites, we further carried out depletions of p60 in combination with either HIRA or DAXX. We checked all depletion efficiencies (Figure 3C) and that the number of EdU-positive cells remained comparable (Figure S3B). Codepletion of p60 and HIRA reduced this 20% of cells to 5% while 15% still remained after codepletion of p60 and

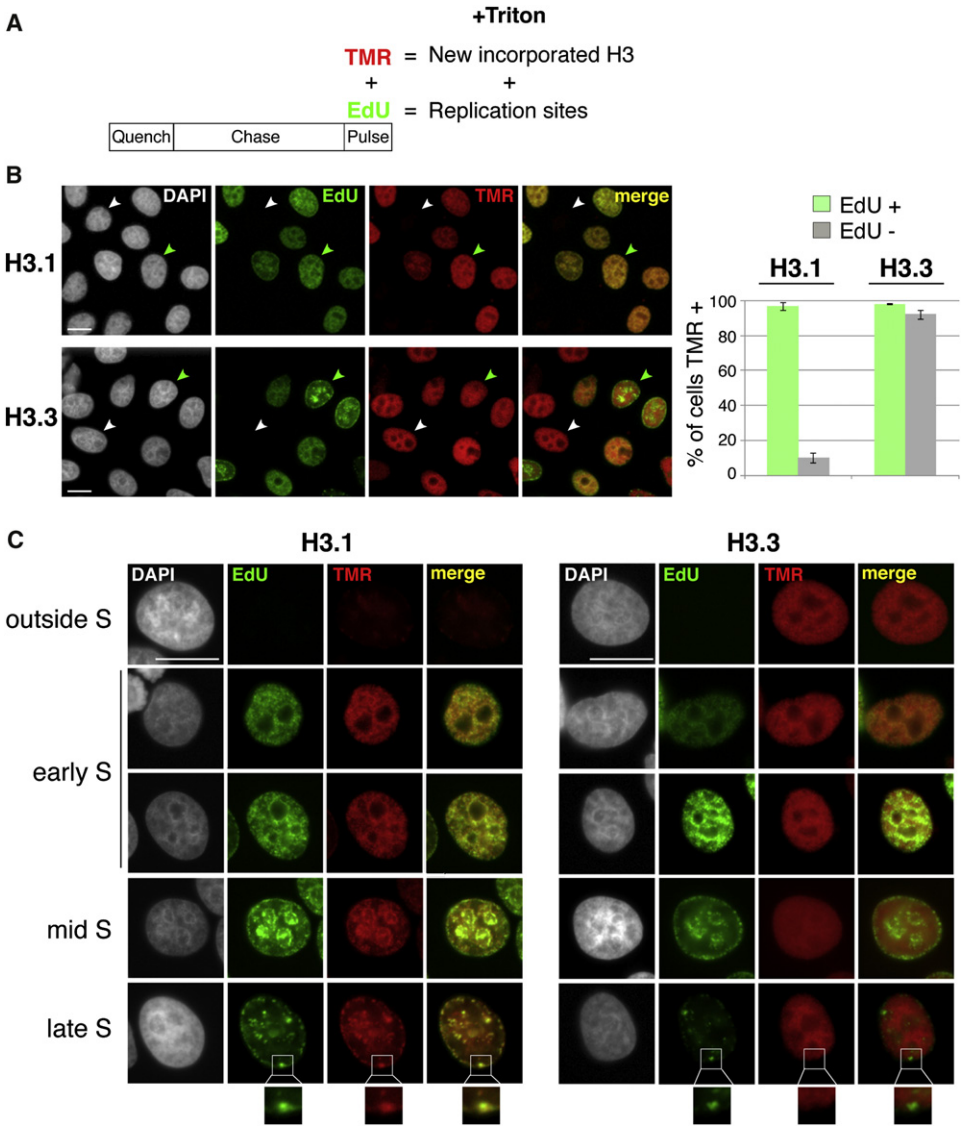

Figure 2. Newly Deposited H3.1 Overlaps with the Replication Sites In Vivo, while H3.3 Does Not

(A) Scheme of the assay for in vivo labeling new incorporated H3.1 and H3.3 by the quench-chase-pulse experiment and replication sites with EdU. Cells are treated with triton before fixation to visualize incorporated histones only.

(B) Left: Fluorescent microscopy visualization of replication sites (EdU, green) and of new incorporated H3.1 and H3.3 (red) after in vivo labeling. The white and green arrowheads indicate typical negative and positive EdU cells, respectively. Scale bars represent 10 μm. Right: Graph representation of the percentage of H3.1 and H3.3 cells negative (EdU –) or positive (EdU +) for EdU staining which are labeled with TMR-Star. Error bars indicate the standard deviation in at least three experiments.

(C) Fluorescent microscopy visualization of the different patterns of replication sites (EdU, green) during early, mid, or late S phase and of new incorporated H3.1 and H3.3 (red) after in vivo labeling by a quench-chase-pulse experiment. Insets represent enlarged images of selected area. Scale bars represent 10 μm. See also Figure S2.

DAXX. These data favor the HIRA complex as the major player in H3.3 deposition at replication sites when H3.1 deposition is impaired.

In summary, these data show that depletion of CAF-1 p60 impairs incorporation of H3.1 and provides an opportunity for H3.3 to get incorporated at replication sites. This mechanism involving HIRA may provide means to compensate at least in part for chromatin assembly defects.

Depletion of the HIRA Complex Severely Affects the De Novo Deposition of H3.3 without Permitting Significant H3.1 Incorporation throughout the Cell Cycle

We next examined the HIRA complex components, HIRA, UBN1, and Cabin1, and their association with H3.3 and H3.1 (Figure 4A, left). After immunoprecipitation of H3.1 or H3.3 from HeLa nuclear extracts with an anti-HA antibody, we found HIRA, UBN1, and Cabin1 coprecipitating with H3.3 but not with H3.1. In contrast,

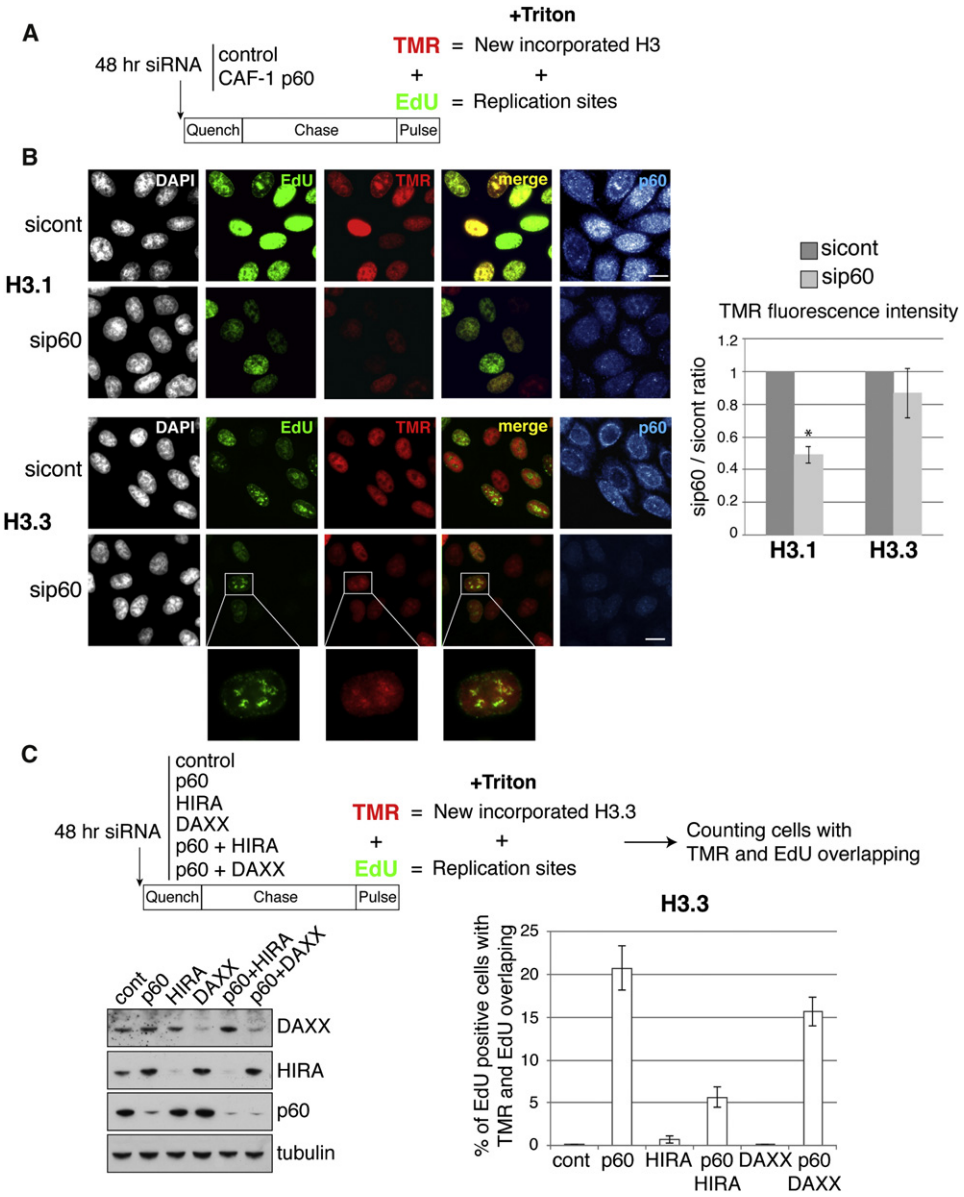

Figure 3. Alternative Deposition of H3.3 at Replication Sites when H3.1 Incorporation Is Impaired by CAF-1 Depletion

(A) Scheme of the assay for labeling new incorporated H3.1 and H3.3 by the quench-chase-pulse experiment and replication sites with EdU during the pulse, coupled with transfection of siRNA against CAF-1 p60 (sip60#1) or control 48 hr before the in vivo labeling.

(B) Left: Fluorescent microscopy visualization of replication sites (EdU, green) and new incorporated H3.1 or H3.3 (red) after siRNA transfection against CAF-1 p60 or control. CAF-1 p60 is detected by immunofluorescence (blue). The insets represent enlarged images of one selected cell. Scale bars represent 10 μm. Right: Graph showing the sip60/sicont ratio corresponding to TMR fluorescence intensity for H3.1 and H3.3. Error bars indicate standard deviation in at least three experiments. A Mann and Whitney statistical test established the significance of the difference between sip60 and sicont (for H3.1 $p = 0.02$ and H3.3 $p = 0.35$).

(C) Top: Scheme of the assay for labeling new incorporated H3.3 by the quench-chase-pulse experiment and replication sites with EdU during the pulse, coupled with transfection of siRNAs before the in vivo labeling. We counted the cells presenting overlapping TMR and EdU signals. Bottom left: Western blotting on total extracts from siRNA-treated cells to verify efficiency of the indicated siRNAs. Bottom right: Graph showing the percentage of EdU positive cells with TMR and EdU overlapping in the indicated siRNA-treated cells. Error bars indicate the standard deviation in at least three experiments.

See also Figure S3.

CAF-1 p60 and p150 subunits specifically coimmunoprecipitated with H3.1. Moreover, antibodies directed against HIRA, UBN1, or Cabin1 coimmunoprecipitated all three proteins in each instance but not CAF-1 p60, confirming that they are part of a common complex (Figure 4A, middle). This complex depends on HIRA since siHIRA-treated cells showed a concommitant decrease of HIRA, UBN1, and, to a lesser extent, Cabin1 (Figure 4A, right) consistent with reports in (Banumathy et al., 2009; Rai et al., 2011).

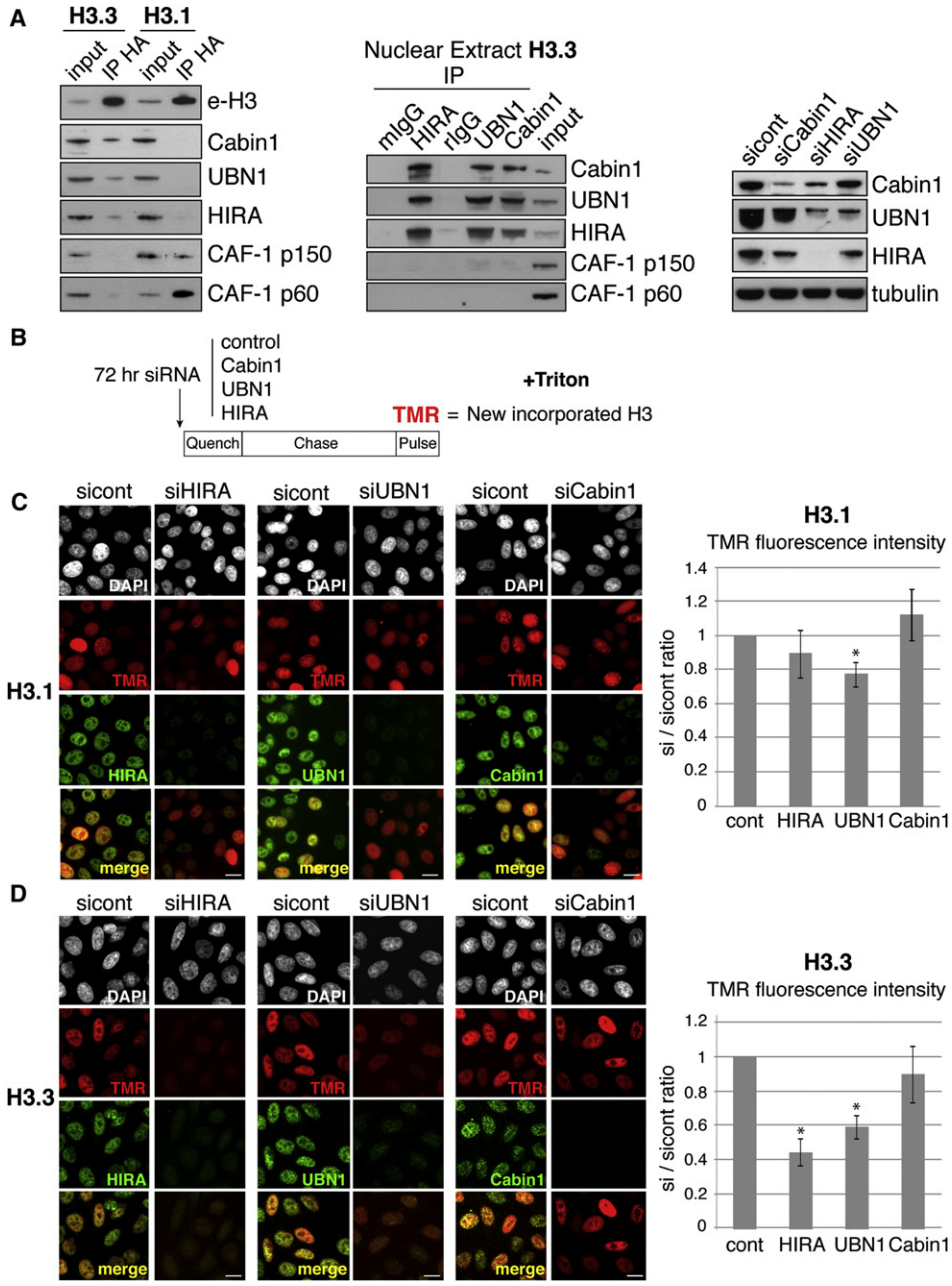

Figure 4. Depletion of the HIRA Complex Severely Affects the De Novo Deposition of H3.3 without Permitting Significant H3.1 Incorporation throughout the Cell Cycle

(A) Western blot analysis of anti-HA immunoprecipitates from nuclear extracts of cells expressing SNAP-tagged H3.1 or H3.3 (left), immunoprecipitates from nuclear extracts of cells expressing H3.3 with antibodies against HIRA, Cabin1, UBN1 or rabbit (rIgG) and mouse (mIgG) IgG controls (middle), and total extracts from cells treated with the indicated siRNAs (right). Input corresponds to 10% of nuclear extract used for each experiment.

(B) Scheme of the assay for labeling new incorporated H3.1 and H3.3 by the quench-chase-pulse experiment coupled with transfection of siRNAs against Cabin1, UBN1, HIRA (siHIRA#1), or control 72 hr before the in vivo labeling.

(C) Left: Fluorescent microscopy visualization of new incorporated H3.1 (red) after treatment with the indicated siRNAs. Cabin1, UBN1, or HIRA are revealed by immunofluorescence (green). Scale bars represent 10 μm. Right: Graph showing the ratio of TMR fluorescence intensity siRNA/sicont for H3.1. Error bars indicate standard deviation in at least three experiments. The statistical significance of the difference between siRNA and sicont was analyzed with a Mann and Whitney test (for siHIRA $p = 0.17$, siUBN1 $p = 0.01$ and siCabin1 $p = 0.35$).

(D) As in (C) but for H3.3. The statistical significance of the difference between siRNA and sicont was analyzed using a Mann and Whitney test (for siHIRA $p = 0.02$, siUBN1 $p = 0.01$ and siCabin1 $p = 0.35$). The statistical significance of the difference between H3.1 and H3.3 was tested using a Mann and Whitney test: for siHIRA $p = 0.02$ and UBN1 $p = 0.05$.

See also Figures S4 and S5.

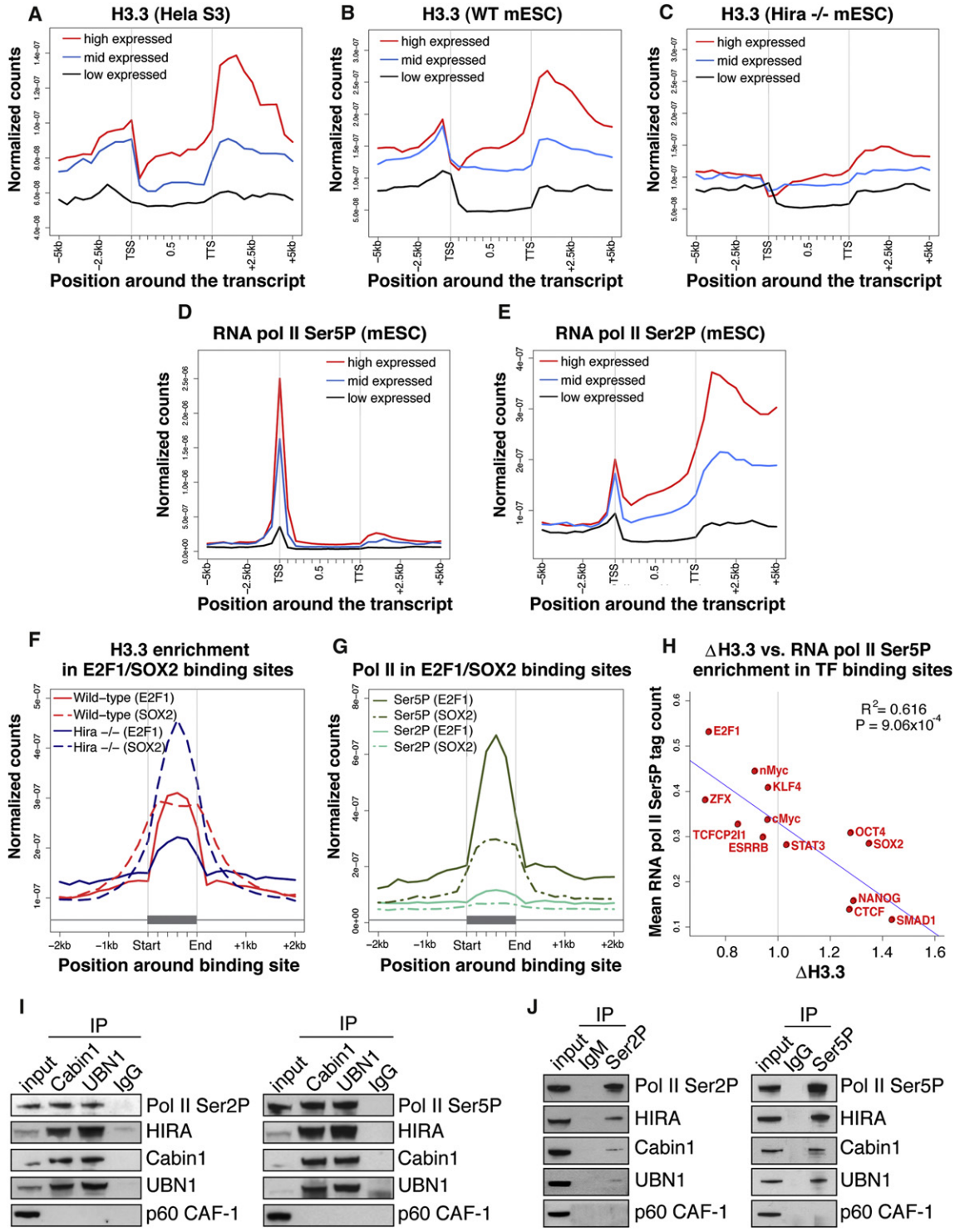

Figure 5. A Link between HIRA Complex-Dependent H3.3 Deposition and RNA pol II

(A–C) ChIP-seq density profiles of histone variant H3.3 in human HeLa S3 cells expressing H3.3-FLAG-HA (A) and wild-type (B) and HIRA$^{-/-}$ (C) mESCs expressing tagged endogenous H3.3, within the gene body and up to 5 kb upstream and downstream of 800 highly expressed (red), medium expressed (blue), and low expressed (black) genes. H3.3 data in mESCs is from Goldberg et al. (2010). TSS, transcription start site; TTS, transcription termination site. Note that we carried out chromatin preparation under high-salt conditions (450 mM NaCl), meaning that we potentially lost the unstable H3.3/H2A.Z double variant known to be enriched at promoters (Jin et al., 2009).

(D and E) ChIP-seq density profiles of RNA pol II Ser5- and Ser2-phosphorylated forms in WT mESCs. RNA pol II data is from Rahl et al. (2010).

We then wished to determine the importance of HIRA, UBN1, and Cabin1 in the deposition of H3.1 and H3.3. For this, we transfected cells expressing H3.1 and H3.3 (scheme Figure 4B) with siRNA against HIRA, Cabin1, or UBN1 prior to the "quench-chase-pulse" experiment. We verified cell cycle profiles by flow cytometry analysis and that the percentage of EdU-positive cells remained comparable in all cases (Figure S4A). Depletion of Cabin1 did not decrease H3.1 incorporation and affected H3.3 deposition by only 10%, as shown by microscopy analysis followed by quantification of TMR fluorescence intensity (Figures 4C and 4D). In HIRA complex- and UBN1-depleted cells we observed 10% and 20% reduction of signal for H3.1, respectively (Figure 4C). In contrast, the effect on TMR fluorescence intensity was significantly stronger for H3.3 with a decrease of about 55% and 40% in HIRA complex- and UBN1-depleted cells, respectively (see Figure 4D and statistics). Interestingly, we could not detect nuclei with a broad H3.1 incorporation in siHIRA- or siUBN1-treated cells indicating that H3.1 deposition remains restricted when affecting H3.3 deposition. Using the same assay, we found that DAXX and ATRX depletions did not affect H3.3 deposition (Figure S5). However, we do not exclude other role for DAXX and ATRX in H3.3 deposition at particular loci as telomeres and centromeres that would not be detected in our assay. We confirmed these conclusions, with other siRNAs, against HIRA (siHIRA#2) (Figure S4B) and UBN1 (data not shown), and by comparing cytosolic, nuclear, and chromatin fractions (Figures S4C–S4D).

Altogether our data demonstrate that the HIRA complex is involved in the de novo deposition of H3.3 in vivo. While Cabin1 seems to play an auxilliary role in our deposition assay, depletion of the HIRA complex and to a lesser extent UBN1 alone has a dominant effect on the incorporation of newly synthesized H3.3 in vivo without unleashing massive H3.1 incorporation outside S phase.

A Link between HIRA Complex-Dependent H3.3 Deposition and RNA Polymerase II

The HIRA-dependent enrichment of H3.3 in the body of transcribed genes and at CpG island promoters of both transcribed and repressed genes in mouse ESCs (Goldberg et al., 2010) suggests that H3.3 deposition may be linked to transcription. Here, in human HeLa cells expressing H3.3-FLAG-HA (Tagami et al., 2004), we carried out a ChIP-seq of H3.3 for a systematic comparison with a previously generated H3.3 dataset in mouse ESCs (mESCs) expressing tagged endogenous H3.3 (Goldberg et al., 2010). In HeLa cells, we find a distinct H3.3 density profile in and around highly transcribed genes (Figure 5A) consistent with previous findings (Jin et al., 2009), which is almost identical in mESCs (Figure 5B). This suggests a mechanism for H3.3 deposition in transcribed genes that is conserved across species and cell types. In the absence of HIRA, the H3.3 density pattern is largely lost in mESCs (Figure 5C) (Goldberg et al., 2010), confirming the importance of HIRA in H3.3 enrichment at these sites. RNA pol II large subunit is regulated by phosphorylation of its carboxy terminal repeats, phosphorylation at Ser5 being associated with transcription initiation while its phosphorylation at Ser2 occurs during elongation (Brookes and Pombo, 2009; Buratowski, 2009). Notably, the direct comparison of this H3.3 density profile with ChIP-seq data of Ser5P and Ser2P forms of RNA polymerase II (RNA pol II) in mESCs (Rahl et al., 2010), across the same set of transcripts, displayed a highly similar profile to that seen for H3.3 (Figures 5D and 5E). Together, these enrichment profiles for the two modified forms of RNA pol II thus provide correlative evidence that the presence RNA pol II at a specific genomic locus directly increases the likelihood of H3.3 enrichment, in a HIRA-dependent fashion.

In addition to transcriptional units, H3.3 was found enriched at intergenic *cis*-regulatory elements in mESCs (Goldberg et al., 2010). In the same study, only a third of these sites had significantly reduced H3.3 levels when HIRA was knocked out, suggesting that H3.3 deposition at many regulatory elements is not HIRA dependent. We thus investigated closer whether the correlation between HIRA-dependent H3.3 deposition and the presence of RNA pol II also held true at these distal *cis*-regulatory elements. Using a set of genome-wide intergenic binding sites for 13 transcription factors in mESCs (Chen et al., 2008), we measured the mean change in H3.3 enrichment in wild-type and HIRA-deficient cells for each set of binding sites and found that the extent of this change differs significantly between factors. For example, E2F1 and SOX2 binding sites have similar levels of mean H3.3 in their binding sites in wild-type mESCs, but in HIRA-deficient cells, E2F1 binding sites show an overall reduction of H3.3, while SOX2 sites show an increase (Figure 5F and Figure S6). Interestingly, we found that the level of

(F and G) ChIP-seq density profiles for H3.3 and RNA pol II (Ser5- and Ser2-phosphorylated forms) within, and up to 2 kb on either side of, intergenic binding sites for two representative factors, E2F1 and SOX2, active in mESCs. Binding sites were identified with ChIP-seq data from Chen et al. (2008). SOX2 binding sites show an increase of H3.3 level in HIRA-deficient cells as compared to wild-type mESCs that is likely an artifact of the reduction in HIRA-dependent transcription factor sites rather than an absolute increase in the level of H3.3 enrichment, as there is now a redistribution of a similar number of total sequence reads across a smaller number of HIRA-independent transcription factor sites. The ChIP-seq enrichment of Pol II we detect at most of these binding factors may reflect active transcription recently shown to play a role in enhancer function (Mattick, 2010), although the predominant enrichment of Pol II Ser5P suggests it is more likely to be the capturing of looped enhancer-promoter interactions during the crosslinking step of the ChIP.

(H) Mean levels of RNA pol II Serine 5 inside the intergenic binding sites is correlated with ΔH3.3, a measure of the change in mean levels of H3.3 within binding sites between wild-type and HIRA deficient mESCs (see the Experimental Procedures). Values below 1 (gray line) represent a greater proportion of sites dependent on HIRA mediated H3.3 deposition, while those above 1 represent a lower proportion.

(I) Western blot analysis of immunoprecipitates from nuclear HeLa extracts with antibodies against Cabin1, UBN1, or rabbit IgG control showing the coimmunoprecipitation of RNA polymerase II phosphorylated at Ser2 (left) and at Ser5 (right). Input corresponds to 10% of nuclear extract used for each experiment.

(J) Western blot analysis of immunoprecipitates from HeLa nuclear extracts with specific antibodies against RNA polymerase II Ser2P and its mouse IgM control (left) or RNA polymerase II Ser5P and its mouse IgG control (right) showing that both RNA pol II antibodies coimmunoprecipitated Cabin1, UBN1 and HIRA. Input corresponds to 10% of nuclear extract used for each experiment.

See also Figure S6.

enrichment of RNA pol II Ser5P (but not Ser2P) also differs significantly within the binding sites of these factors (Figure 5G). Across all 13 factors, we found a significant correlation ($R^2 = 0.616$, $p = 9.06 \times 10^{-4}$) between the mean level of RNA pol II Ser5P and overall HIRA dependency of H3.3 within the binding site (Figure 5H and Figure S6). Thus, we find that the higher the mean level of RNA pol II Ser5P, the higher the mean level of HIRA-dependent H3.3 enrichment at transciption factor binding sites. This is further confirmed by the observation that the level of H3.3 enrichment at binding sites is also correlated with the presence of Pol II, but only in the presence of HIRA (Figure S6). These results suggest that the presence of RNA pol II at regulatory elements can at least partly explain why some regulatory elements have more HIRA-dependent H3.3 enrichment than others.

This correlation between the HIRA-dependent enrichment of H3.3 and RNA pol II prompted us to ask whether the HIRA complex is associated with the transcriptional machinery, in particular with the largest subunit of RNA pol II. Cabin1 and UBN1 antibodies coimmunoprecipitated both phosphorylated forms of RNA pol II with specific antibodies recognizing either Ser2- or Ser5-phosphorylated RNA pol II (Stock et al., 2007), but not CAF-1 p60 (Figure 5I). The reverse immunoprecipitation experiments showed that both Ser2P and Ser5P RNA pol II antibodies coimmunoprecipitated the three components of the HIRA complex, Cabin1, UBN1, and HIRA, but not CAF-1 p60 (Figure 5J).

From these results, we conclude that HIRA-dependent H3.3 enrichment at genes and a subset of regulatory elements correlates with the presence of RNA pol II and that the HIRA complex associates with both the promoter-associated and the elongating forms of RNA pol II in vivo.

The HIRA Complex Binds Directly to DNA and Its Depletion Increases DNase Sensitivity

While the association of the HIRA complex with RNA pol II can explain the H3.3 enrichment at genes and a subset of regulatory elements, the observation of H3.3 incorporation at replication sites when H3.1 deposition is impaired (Figure 3) indicates that at least some H3.3 incorporation likely occurs independently of RNA pol II. This is further underscored by the large-scale transcription-independent HIRA-mediated H3.3 deposition in the male pronucleus after fertilization (Loppin et al., 2005; Torres-Padilla et al., 2006; van der Heijden et al., 2005), indicating the possibility of an alternative mode of targeting. A common feature in both cases is the exposure of nonnucleosomal/naked DNA, which thus potentially represents a direct target for HIRA-mediated H3.3 deposition. One can therefore envisage, in the simplest scenario, that this is promoted by a capacity of the HIRA complex to bind naked DNA. To test this hypothesis, using plasmid DNA fixed on magnetic beads, we found that HIRA, UBN1, and Cabin1 from nuclear extracts could readily bind DNA in contrast to any of the other histone chaperones examined in parallel (Figure 6A). This includes p48, p60, and p150 subunits of CAF-1, Asf1a/b, and NASP that have been identified in both H3.1 and H3.3 complexes (Tagami et al., 2004), spt6 and spt16 (FACT subunit), known to be linked with the transcriptional machinery (Sims et al., 2004), DEK, ATRX, and DAXX. Furthermore, RNA pol II (Ser5P and Ser2P) exhibited only low DNA binding in these conditions, arguing that the binding of the HIRA complex to DNA is likely independent of RNA pol II. We thus further tested whether a reconstituted recombinant HIRA complex could indeed bind to DNA directly. Our data in Figure 6B confirmed that the HIRA complex on its own also showed direct DNA binding ability without any apparent sequence specificity. Furthermore, each recombinant proteins individually UBN1, Cabin1, and HIRA, could all bind DNA directly in contrast with Asf1a (Figure 6C). An attractive hypothesis is thus that any destabilized nucleosomal DNA region could represent targets for the HIRA complex to reset a nucleosomal organization. In this scheme, one would thus expect that HIRA depletion should lead to an increased genome accessibility. We used DNase digestion on nuclei from siHIRA- and sicont-treated cells and compared the resulting products after gel analysis. The digestion profiles obtained for two separate sets of siRNA showed a higher proportion of smaller fragments in the nuclei from siHIRA-treated cells when compared to control sample (Figure 6D).

We conclude that the HIRA complex is unique among the other H3-H4 histone chaperones tested in exhibiting an ability to directly bind naked DNA. Furthermore, the increased DNase sensitivity observed in HIRA complex-depleted cells argues that nonnucleosomal/naked DNA should be considered as a valid target for a nucleosome gap-filling mechanism at any place in the genome. Taken together, this reveals a protective role leading to a broad incorporation of H3.3 throughout the genome.

DISCUSSION

Our comprehensive analysis of H3.1 and H3.3 deposition in vivo provides a view for the interrelation between CAF-1 and HIRA-mediated pathways to contribute to unique chromatin landscapes as depicted in our model (Figure 7). The CAF-1-mediated H3.1 deposition pathway is strictly limited to sites of DNA synthesis and does not replace the incorporation of H3.3 throughout the cell cycle. The HIRA complex plays a major role in H3.3 deposition throughout the cell cycle and can introduce H3.3 at replication sites when replicative H3.1 incorporation is impaired. The DNA binding ability of the HIRA complex and DNase sensitivity in HIRA-depleted cells unveils a potential nucleosome gap-filling mechanism for HIRA-dependent H3.3 deposition apparently without any sequence specificity. Furthermore, its association with Pol II may aid the targeting of H3.3 to sites of transcription or regulatory elements.

Balance between CAF-1-Dependent H3.1 Deposition and HIRA-Dependent H3.3 Deposition In Vivo

The original model of a replication-coupled (RC) mechanism for canonical H3.1 deposition and both RC and replication-independent (RI) mechanisms for H3.3 deposition was based on early reports in *Drosophila* cells (Ahmad and Henikoff, 2002). Here, beyond confirming this general view, we further provide mechanistic insights into specific targeting and dynamics of deposition involving the CAF-1 and HIRA histone chaperones. First, we reveal that, during S phase, deposition of newly synthesized H3.1 colocalizes with the replication sites in a DNA synthesis-coupled (DSC) manner, whereas newly synthesized H3.3 is excluded from sites of DNA synthesis under normal

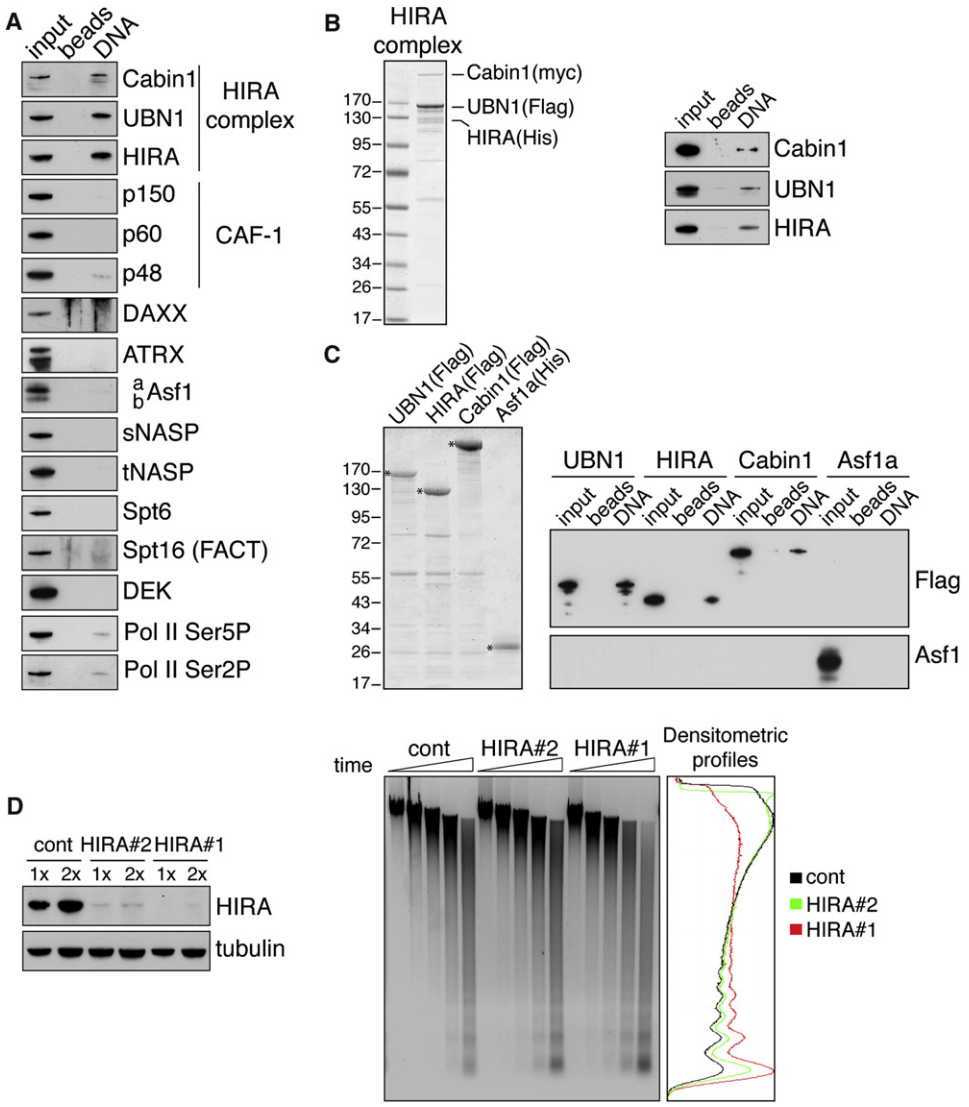

Figure 6. The HIRA Complex Binds Directly to DNA and Its Depletion Increases DNase Sensitivity

(A) Western blot analysis of DNA binding assay using nuclear extracts from HeLa cells. Input corresponds to 50% of nuclear extract used for the experiment.

(B) Left: Recombinant HIRA complex analyzed by NuPAGE and Coomassie stain. Right: Western blot analysis of DNA binding assay using the HIRA complex. Input corresponds to 100% of HIRA complex used for the experiment.

(C) Left: UBN1, HIRA, Cabin1, and Asf1a recombinant proteins analyzed by NuPAGE and Coomassie stain. Right: Western blot analysis of DNA binding assay using each protein individually. Input corresponds to 50% of protein used for the experiment.

(D) Left: Assessment of the efficiency of 96 hr siRNAs treatment against HIRA by western blotting of total extracts. Right: Analysis of the DNase-digestion products (time 0, 30 s, 1 min, 2 min, and 5 min) carried out on nuclei isolated from siHIRA- or sicont-treated cells (total DNA). Densitometric profiles of the 5 min digestion products are shown. Profiles are normalized to the peak of maximum intensity.

circumstances. Second, although H3.3 can be incorporated during S phase, this process is DNA synthesis-independent (DSI) as long as the H3.1 deposition pathway is intact.

Moreover, after downregulation of the histone chaperone CAF-1 p60, a significant number of cells exhibited a deposition pattern for H3.3 that overlapped with EdU labeling. Thus, these cells are able to switch to H3.3 deposition onto replicating DNA when H3.1 cannot be incorporated. Importantly, the fact that the codepletion of p60 and HIRA decreased the number of cells exhibiting newly incorporated H3.3 at replication sites makes the HIRA complex a prime candidate for this H3.3 alternative mechanism. To which extent this alternative mechanism can be compensatory remains to be established. Interestingly, the use of H3.3 in an alternative pathway is consistent with the fact that high H3.3 expression in the protozoa Tetrahymena allows growth in the absence of canonical H3 (Cui et al., 2006). Our data however, do not support the use of H3.1 in place of H3.3 as a converse alternative mechanism, perhaps because our system does not overproduce H3.1. Again, this is supported in Tetrahymena, where cells deficient in H3.3 cells do not use

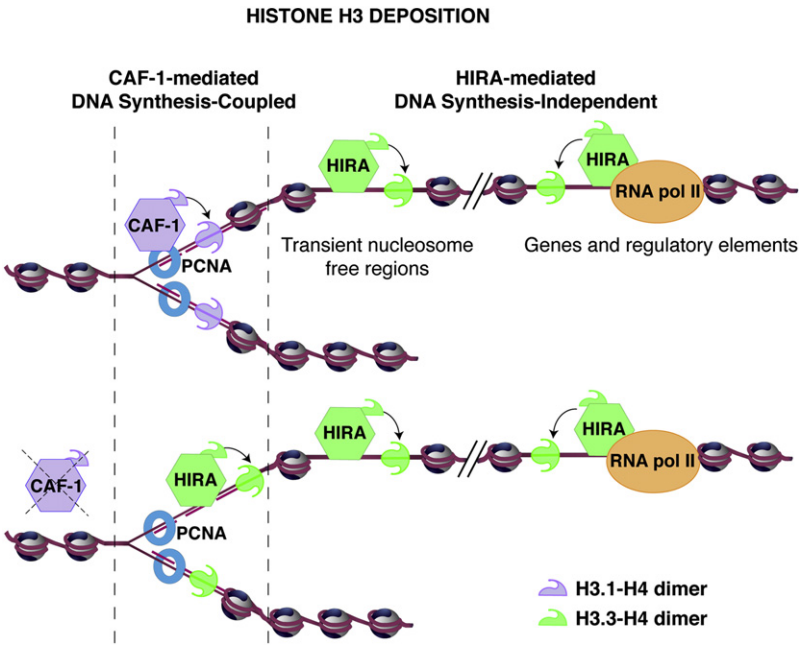

Figure 7. Model for Histone H3 Deposition

Model for CAF-1-mediated DNA synthesis-coupled (DSC) and HIRA complex-mediated DNA synthesis-independent (DSI) histone H3 deposition. CAF-1 mediates H3.1 deposition through its interaction with PCNA during replication (and DNA repair) while the HIRA complex mediates H3.3 deposition broadly through binding to transient accessible non nucleosomal DNA during postreplication, sperm reprogramming, and any event generating transient naked DNA. In regions associated with RNA pol II (promoters, coding regions, and a subset of *cis*-regulatory elements), the interaction between the HIRA complex and RNA pol II facilitates H3.3 deposition. When CAF-1 is depleted and therefore H3.1 deposition is impaired, the HIRA complex enables alternative H3.3 incorporation at nonnucleosomal DNA at sites of synthesis.

canonical H3 for DSI assembly even in absence of H3.3 (Cui et al., 2006). This unidirectional replacement/alternative mechanism may therefore reflect a conserved and possibly ancient function of H3.3 (Szenker et al., 2011). Intriguingly, in flies deficient for H3.3, canonical H3 gets overexpressed and incorporates in a DSI manner (Sakai et al., 2009), suggesting some parsimonious function of the deposition pathways. If such a mechanism occurs in our system, without massive unbalancing of H3 variants, it remains beyond our detection limits. Furthermore, these overall data suggest that the limiting step is whether the actual deposition pathways can be targeted where it is needed.

Together our data emphasize the possibility of H3.3 incorporation via HIRA at replication sites when H3.1 deposition is impaired. This finding reflects a potential for restoration of nucleosomal organization during replication using any available H3 variants to ensure maintenance of chromatin stability.

HIRA Is a Major Histone Chaperone Complex Involved in H3.3 Deposition In Vivo

Our deposition assay demonstrates that HIRA, as a complex, is a critical actor in the incorporation of H3.3 throughout the cell cycle with a broad genome coverage. Remarkably, the defect in H3.3 deposition after UBN1 downregulation indicates that the sole presence of HIRA and Cabin1 is not sufficient for efficient H3.3 incorporation. The stronger defect with siRNA treatment against HIRA further underlines the importance of HIRA and the overall complex. Indeed, we found that the presence of HIRA is important for the stability of UBN1 and Cabin1, providing further evidence for their role as a complex. The most striking defects in H3.3 deposition in both nonreplicating and replicating cells after siHIRA and siUBN1 treatment demonstrate their critical role for H3.3 deposition both during and outside S phase. The role of Cabin1, given that its downregulation did not significantly affect H3.3 deposition may be in controlling the availability of H3.3 rather than its actual deposition as suggested by the increased amount of soluble H3.3 in Cabin1-downregulated cells (Figure S4D). It is noteworthy that no ortholog of this subunit has been identified in *Drosophila* so far. Taken together, we conclude that HIRA is a central component for the function of the complex to ensure H3.3 deposition throughout the cell cycle.

HIRA-Dependent H3.3 Deposition at Pol II Sites

The enrichment of the histone variant H3.3 at transcriptionally active regions in various metazoans (Goldberg et al., 2010; Jin et al., 2009; Mito et al., 2005) and the dependency of this on HIRA in mouse ESCs suggests a close association between HIRA and the transcriptional machinery. In support of this, we found that the HIRA complex associates with both initiating (Ser5P) and elongating (Ser2P) forms of RNA pol II in vivo. Whether the HIRA-Pol II interaction is direct or mediated by another component of the transcriptional machinery remains to be addressed. Furthermore, this association is also strongly supported by striking similarities in ChIP-seq enrichment profiles of H3.3 and Pol II in transcribing regions, at the promoter and downstream of the TTS. These are regions where Pol II is known to be paused for significant periods of time, during Ser5P initiation at the promoter, or 0.5–1.5 kb downstream of the TTS where Ser2P recruits 3′ processing factors (Core and Lis, 2008; Glover-Cutter et al., 2008). Remarkably, the correlation of HIRA-dependent H3.3 deposition and Pol II remains true even in intergenic regulatory regions corresponding to specific transcription factor binding sites. Thus, these data suggest an important role for the association of Pol II and HIRA in promoting local H3.3 enrichment.

HIRA-Dependent H3.3 Deposition by Nucleosome Gap Filling

In addition to targeted local deposition, we discovered that the HIRA complex can bind to naked DNA, whereas the other histone chaperones that we tested did not. This uncovers an alternative mode of HIRA dependent H3.3 deposition at any region where nonnucleosomal/naked DNA is accessible, that

could differ from one cell to the next and thus would not have been picked up in analyzing genome-wide H3.3 enrichment profiles. This is supported by the higher sensititivity observed in our assay for DNA accessibility using DNase digestion on nuclei isolated from cells depleted of the HIRA complex. Thus H3.3 distribution is not simply reflecting active transcription but rather reflects the deposition pathway available. This could explain how HIRA participates in large-scale deposition of H3.3 on the paternal pronucleus after fertilization in *Drosophila* (Loppin et al., 2005) and in mouse embryos (Santenard et al., 2010; Torres-Padilla et al., 2006; van der Heijden et al., 2005). Interestingly, the yeast homolog of the HIRA complex as well as Yemanuclein, the *Drosophila* homolog of UBN1, also exhibit DNA binding ability, suggesting that this is a conserved property (Aït-Ahmed et al., 1992; Prochasson et al., 2005). Furthermore, HIRA, UBN1, and Cabin1 recombinant proteins bound DNA individually in vitro, indicating that each of them may participate in targeting the HIRA complex for H3.3 deposition in vivo. In contrast, H3.3 chaperones ATRX and DAXX do not exhibit significant levels of binding to random DNA, but ATRX is known to show a preference for sequences capable of forming a G quadruplex (Law et al., 2010), a property that could contribute to their specific targeting to telomeres and pericentric heterochromatin (Drané et al., 2010; Goldberg et al., 2010).

In conclusion, the HIRA complex provides a nucleosome gap-filling strategy that may operate in all instances, although the interaction of the HIRA complex with Pol II may provide additional targeting. H3.3 deposition by HIRA at naked DNA may be part of a salvage pathway that acts to avoid leaving nucleosome-free DNA regions. This mechanism might be especially critical after DNA replication to prevent chromatin defects at the level of the nucleosomal structure for instance during rapid divisions in early development (Ray-Gallet et al., 2002) or to control unwanted cryptic transcription (Anderson et al., 2010). Evaluating to which extent the use of the alternative pathway fully restores preexisting function will be important in particular during development when specific marking have to be set in place. Finally, it will be of interest to investigate whether challenges to nucleosomal organization may make cells more dependent on such a protective pathway, during stress or DNA damage and according to developmental context.

EXPERIMENTAL PROCEDURES

Human Cell Lines

We established cell lines stably expressing H3.1-SNAP-3XHA or H3.3-SNAP-3XHA in HeLa cells. The H3.1 or H3.3 open reading frames (ORFs) were amplified from complementary DNA by PCR and cloned between the KpnI/XhoI sites of pCENP-A-SNAP-3XHA (Jansen et al., 2007) replacing the CENP-A gene. The resulting H3.1-SNAP-3XHA or H3.3-SNAP-3XHA ORFs were subcloned into pBABE and used for retroviral production and delivery into HeLa cells essentially as described previously (Shah et al., 2004). We selected them by Blasticidin S (5 μg/ml; Calbiochem) and isolated monoclonal lines by flow cytometry. We verified the low expression levels of tagged H3.1 and H3.3 as compared to the endogenous counterparts to be able to use them as tracers (data not shown).

H3-SNAP Labeling In Vivo

The SNAP labeling protocol is as described (Jansen et al., 2007). We added to cell medium at 37°C 10 μM SNAP-Cell Block (Biolabs) during 30 min to quench SNAP-tag activity or 2 μM of SNAP-Cell TMR-Star (Biolabs) during 20 min for pulse labeling. After washing of cells with prewarmed PBS, reincubation in complete medium for 30 min allowed excess compound to diffuse from cells and then cells were washed again in PBS. For the chase, incubation of cells was for 2 hr in complete medium at 37°C. After in vivo labeling, the cells (with or without triton pre-extraction) were either directly used for SNAP labeling visualization by microscopy or processed for immunostaining. Alternatively, we harvested cells in Laemmli buffer (with or without triton pre-extraction) to prepare cell extracts for NuPAGE bis-tris 4%–12% gel migration in MOPS buffer (Invitrogen) and fluorescence visualization in gel with a Typhoon FLA 9000 (GE Healthcare-Life Sciences). Fluorescence signal was estimated using ImageJ software after normalization using Coomassie staining.

Microscopy Analysis and Quantification of TMR Signal

To quantify fluorescence intensity (TMR signal) in the acquired images, we used the ImageJ software. We first defined background fluorescence by measuring the mean gray value (gray value divided by the area) from an area containing no nucleus. We then subtracted this general background in each image and quantified the mean gray value in each nucleus, that we called "fluorescence intensity." Only TMR-positive nuclei were subjected to this quantification on series of at least 100 and 300 nuclei for H3.1 and H3.3, respectively (mean = 397 ± 33 for H3.1 and 479 ± 36 for H3.3) in each experiment. The average fluorescence intensity was calculated for each condition in each experiment and normalized to sicont. At least, three independent experiments were performed for each siRNA condition and we applied a Mann and Whitney statistical test with the R software.

Immunofluorescence and Replication Sites Visualization

We carried out pre-extraction of cells prior to fixation for 5 min with 0.5% Triton in CSK buffer (10 mM PIPES [pH 7], 100 mM NaCl, 300 mM sucrose, 3 mM $MgCl_2$) in the presence of protease inhibitors as in (Martini et al., 1998), and we fixed cells in 2% paraformaldehyde. Non-pre-extracted cells were permeabilized 5 min with 0.2% Triton in PBS. We blocked cells with BSA (5% in PBS plus 0.1% Tween) before incubation with primary and secondary antibodies and DAPI staining. Coverslips were mounted in Vectashield medium. We used a Leica widefield microscope (40× objective).

We labeled replication sites in vivo by a 20 min EdU pulse concomitantly with the TMR-Star pulse. We visualized EdU with the Click-iT EdU Alexa Fluor 488 imaging kit (Invitrogen) on cells pre-extracted or not with Triton before fixation. EdU, which is a nucleoside analog of thymidine, incorporates into DNA during active DNA synthesis in vivo. Contrary to BrdU, EdU detection does not require DNA denaturation for its detection and thus preserves TMR-Star fluorescence. EdU detection can be followed by immunofluorescence using the above-described protocol.

H3.3 ChIP and ChIP-Seq

We performed mononucleosome purification from the HeLa S3 H3.3-FLAG-HA cell line as in Loyola et al. (2006) and recovered immunoprecipitated DNA after proteinase K digestion and phenol chloroform extraction, followed by ethanol precipitation. We used 100 ng of DNA for library preparation and performed DNA sequencing on an Illumina GA IIx by Fasteris-SA (Ch. du Pont-du-Centenaire 109 CH-1228 Plan-les-Ouates Switzerland) after the Illumina protocol.

ChIP-Seq Data Analysis

We analyzed a number of previously published ChIP-seq datasets in mouse ESCs: HA-tagged H3.3 in wild-type and $HIRA^{-/-}$ cells (Goldberg et al., 2010), H3K4me3 and H3K4me1 (Goldberg et al., 2010), H3K27ac (Creyghton et al., 2010), H3K27me3 (Rugg-Gunn et al., 2010), RNA Pol II Ser5P and Ser2P (Rahl et al., 2010), and 13 transcription factors (cMyc, CTCF, E2F1, ESRRB, KLF4, NANOG, nMyc, OCT4, SOX2, STAT3, TCFCP2l1, and ZFX) together with a GFP control (Chen et al., 2008). The HeLa H3.3 ChIP-seq was mapped in the same way to the human genome (assembly Hg18).

See also the Supplemental Information.

Purification of Recombinant Proteins

The recombinant trimeric complex HIRA(His)-UBN1(Flag)-Cabin1(myc) and individual proteins HIRA(Flag), UBN1(Flag), Cabin1(Flag), and His-Asf1a

were expressed in baculovirus infected Sf9 and purified as described in the Supplemental Information.

DNA Binding Assay

Bead-linked plasmid DNA (PUC19) substrate was obtained as previously described (Mello et al., 2004). Mock-beads or DNA beads were blocked with BSA (1 mg/ml) and incubated 1 hr at 30°C with 20 μg of HeLa nuclear extracts or ≈200 ng of recombinant proteins in buffer containing 10 mM HEPES (pH 7.8), 2 mM $MgCl_2$, 1mM $CaCl_2$, 0.5 mM EGTA, 100 mM NaCl, 0.1% NP40, and 8% glycerol in a final volume of 50 μl. Then, the beads were washed three times in the presence of 300 mM NaCl and 0.5% NP40. Bound proteins were analyzed by Western blot.

Digestion of Nuclei with DNase

We carried out digestion with DNase (RQ1, Promega) on nuclei isolated from 96 hr siRNA-treated HeLa H3.3-SNAP cells. Digestion products were analyzed by agarose gel electrophoresis followed by ethidium bromide staining for visualizion with a Typhoon FLA 9000 (GE Healthcare-Life Sciences). Plot profiles were obtained with ImageJ software.

ACCESSION NUMBERS

Our HeLa S3 H3.1/H3.3 ChIP-seq data sets have been deposited in the GEO database with the accession number GSE31794.

SUPPLEMENTAL INFORMATION

Supplemental Information includes Supplemental Experimental Procedures and six figures and can be found with this article online at doi:10.1016/j.molcel.2011.12.006.

ACKNOWLEDGMENTS

We thank Sylvain Cantaloube for the macro to quantify fluorescence, Danièle Roche for technical support, Jean-Pierre Quivy for helpful discussions, and Sophie Polo for critical reading. This work was supported by la Ligue Nationale contre le Cancer (Equipe labellisée Ligue 2010), PIC Programs, the European Commission Network of Excellence EpiGeneSys (HEALTH-F4-2010-257082), the European Commission ITN FP7-PEOPLE-2007-215148 "Image DDR" and FP7-PEOPLE-2008-238176 "Nucleosome 4D," ERC Advanced Grant 2009-AdG_20090506 "Eccentric," the European Commission large-scale integrating project FP7_HEALTH-2010-259743 "MODHEP," ANR "ECenS" ANR-09-BLAN-0257-01, ANR "ChromaTin" ANR-10-BLAN-1326-03, and INCa "GepiG." The lab of P.D.A. is funded by NIA program project P01 AG031862. L.E.T.J. was supported by the Fundação Calouste Gulbenkian, Fundação para a Ciência e a Tecnologia (FCT) grant BIA-PRO/100537/2008, the European Commission FP7 programme, and an EMBO installation grant.

Received: May 17, 2011
Revised: November 15, 2011
Accepted: December 6, 2011
Published: December 22, 2011

REFERENCES

Ahmad, K., and Henikoff, S. (2002). The histone variant H3.3 marks active chromatin by replication-independent nucleosome assembly. Mol. Cell *9*, 1191–1200.

Aït-Ahmed, O., Bellon, B., Capri, M., Joblet, C., and Thomas-Delaage, M. (1992). The yemanuclein-alpha: a new Drosophila DNA binding protein specific for the oocyte nucleus. Mech. Dev. *37*, 69–80.

Amin, A.D., Vishnoi, N., and Prochasson, P. (2011). A global requirement for the HIR complex in the assembly of chromatin. Biochim. Biophys. Acta, in press. Published online July 23, 2011.

Anderson, H.E., Kagansky, A., Wardle, J., Rappsilber, J., Allshire, R.C., and Whitehall, S.K. (2010). Silencing mediated by the Schizosaccharomyces pombe HIRA complex is dependent upon the Hpc2-like protein, Hip4. PLoS ONE *5*, e13488.

Balaji, S., Iyer, L.M., and Aravind, L. (2009). HPC2 and ubinuclein define a novel family of histone chaperones conserved throughout eukaryotes. Mol. Biosyst. *5*, 269–275.

Banumathy, G., Somaiah, N., Zhang, R., Tang, Y., Hoffmann, J., Andrake, M., Ceulemans, H., Schultz, D., Marmorstein, R., and Adams, P.D. (2009). Human UBN1 is an ortholog of yeast Hpc2p and has an essential role in the HIRA/ASF1a chromatin-remodeling pathway in senescent cells. Mol. Cell. Biol. *29*, 758–770.

Brookes, E., and Pombo, A. (2009). Modifications of RNA polymerase II are pivotal in regulating gene expression states. EMBO Rep. *10*, 1213–1219.

Buratowski, S. (2009). Progression through the RNA polymerase II CTD cycle. Mol. Cell *36*, 541–546.

Chen, X., Xu, H., Yuan, P., Fang, F., Huss, M., Vega, V.B., Wong, E., Orlov, Y.L., Zhang, W., Jiang, J., et al. (2008). Integration of external signaling pathways with the core transcriptional network in embryonic stem cells. Cell *133*, 1106–1117.

Core, L.J., and Lis, J.T. (2008). Transcription regulation through promoter-proximal pausing of RNA polymerase II. Science *319*, 1791–1792.

Corpet, A., and Almouzni, G. (2009). Making copies of chromatin: the challenge of nucleosomal organization and epigenetic information. Trends Cell Biol. *19*, 29–41.

Corpet, A., De Koning, L., Toedling, J., Savignoni, A., Berger, F., Lemaître, C., O'Sullivan, R.J., Karlseder, J., Barillot, E., Asselain, B., et al. (2011). Asf1b, the necessary Asf1 isoform for proliferation, is predictive of outcome in breast cancer. EMBO J. *30*, 480–493.

Creyghton, M.P., Cheng, A.W., Welstead, G.G., Kooistra, T., Carey, B.W., Steine, E.J., Hanna, J., Lodato, M.A., Frampton, G.M., Sharp, P.A., et al. (2010). Histone H3K27ac separates active from poised enhancers and predicts developmental state. Proc. Natl. Acad. Sci. USA *107*, 21931–21936.

Cui, B., Liu, Y., and Gorovsky, M.A. (2006). Deposition and function of histone H3 variants in Tetrahymena thermophila. Mol. Cell. Biol. *26*, 7719–7730.

De Koning, L., Corpet, A., Haber, J.E., and Almouzni, G. (2007). Histone chaperones: an escort network regulating histone traffic. Nat. Struct. Mol. Biol. *14*, 997–1007.

Deal, R.B., Henikoff, J.G., and Henikoff, S. (2010). Genome-wide kinetics of nucleosome turnover determined by metabolic labeling of histones. Science *328*, 1161–1164.

Drané, P., Ouararhni, K., Depaux, A., Shuaib, M., and Hamiche, A. (2010). The death-associated protein DAXX is a novel histone chaperone involved in the replication-independent deposition of H3.3. Genes Dev. *24*, 1253–1265.

Dunleavy, E.M., Almouzni, G., and Karpen, G.H. (2011). H3.3 is deposited at centromeres in S phase as a placeholder for newly assembled CENP-A in G1 phase. Nucleus *2*, 1–12.

Elsaesser, S.J., and Allis, C.D. (2010). HIRA and Daxx constitute two independent histone H3.3-containing predeposition complexes. Cold Spring Harb. Symp. Quant. Biol. *75*, 27–34.

Foltz, D.R., Jansen, L.E., Bailey, A.O., Yates, J.R., 3rd, Bassett, E.A., Wood, S., Black, B.E., and Cleveland, D.W. (2009). Centromere-specific assembly of CENP-a nucleosomes is mediated by HJURP. Cell *137*, 472–484.

Gaillard, P.H., Martini, E.M., Kaufman, P.D., Stillman, B., Moustacchi, E., and Almouzni, G. (1996). Chromatin assembly coupled to DNA repair: a new role for chromatin assembly factor I. Cell *86*, 887–896.

Glover-Cutter, K., Kim, S., Espinosa, J., and Bentley, D.L. (2008). RNA polymerase II pauses and associates with pre-mRNA processing factors at both ends of genes. Nat. Struct. Mol. Biol. *15*, 71–78.

Goldberg, A.D., Banaszynski, L.A., Noh, K.M., Lewis, P.W., Elsaesser, S.J., Stadler, S., Dewell, S., Law, M., Guo, X., Li, X., et al. (2010). Distinct factors control histone variant H3.3 localization at specific genomic regions. Cell *140*, 678–691.

Groth, A., Rocha, W., Verreault, A., and Almouzni, G. (2007). Chromatin challenges during DNA replication and repair. Cell *128*, 721–733.

Jansen, L.E., Black, B.E., Foltz, D.R., and Cleveland, D.W. (2007). Propagation of centromeric chromatin requires exit from mitosis. J. Cell Biol. *176*, 795–805.

Jiao, Y., Shi, C., Edil, B.H., de Wilde, R.F., Klimstra, D.S., Maitra, A., Schulick, R.D., Tang, L.H., Wolfgang, C.L., Choti, M.A., et al. (2011). DAXX/ATRX, MEN1, and mTOR pathway genes are frequently altered in pancreatic neuroendocrine tumors. Science *331*, 1199–1203.

Jin, C., Zang, C., Wei, G., Cui, K., Peng, W., Zhao, K., and Felsenfeld, G. (2009). H3.3/H2A.Z double variant-containing nucleosomes mark 'nucleosome-free regions' of active promoters and other regulatory regions. Nat. Genet. *41*, 941–945.

Kaufman, P.D., and Rando, O.J. (2010). Chromatin as a potential carrier of heritable information. Curr. Opin. Cell Biol. *22*, 284–290.

Keppler, A., Gendreizig, S., Gronemeyer, T., Pick, H., Vogel, H., and Johnsson, K. (2003). A general method for the covalent labeling of fusion proteins with small molecules in vivo. Nat. Biotechnol. *21*, 86–89.

Kouzarides, T. (2007). Chromatin modifications and their function. Cell *128*, 693–705.

Law, M.J., Lower, K.M., Voon, H.P., Hughes, J.R., Garrick, D., Viprakasit, V., Mitson, M., De Gobbi, M., Marra, M., Morris, A., et al. (2010). ATR-X syndrome protein targets tandem repeats and influences allele-specific expression in a size-dependent manner. Cell *143*, 367–378.

Lewis, P.W., Elsaesser, S.J., Noh, K.M., Stadler, S.C., and Allis, C.D. (2010). Daxx is an H3.3-specific histone chaperone and cooperates with ATRX in replication-independent chromatin assembly at telomeres. Proc. Natl. Acad. Sci. USA *107*, 14075–14080.

Loppin, B., Bonnefoy, E., Anselme, C., Laurençon, A., Karr, T.L., and Couble, P. (2005). The histone H3.3 chaperone HIRA is essential for chromatin assembly in the male pronucleus. Nature *437*, 1386–1390.

Loyola, A., Bonaldi, T., Roche, D., Imhof, A., and Almouzni, G. (2006). PTMs on H3 variants before chromatin assembly potentiate their final epigenetic state. Mol. Cell *24*, 309–316.

Martini, E., Roche, D.M., Marheineke, K., Verreault, A., and Almouzni, G. (1998). Recruitment of phosphorylated chromatin assembly factor 1 to chromatin after UV irradiation of human cells. J. Cell Biol. *143*, 563–575.

Mattick, J.S. (2010). Linc-ing Long noncoding RNAs and enhancer function. Dev. Cell *19*, 485–486.

Mello, J.A., Moggs, J.G., and Almouzni, G. (2004). Analysis of DNA repair and chromatin assembly in vitro using immobilized damaged DNA substrates. Methods Mol. Biol. *281*, 271–281.

Mito, Y., Henikoff, J.G., and Henikoff, S. (2005). Genome-scale profiling of histone H3.3 replacement patterns. Nat. Genet. *37*, 1090–1097.

Polo, S.E., and Almouzni, G. (2005). Histone metabolic pathways and chromatin assembly factors as proliferation markers. Cancer Lett. *220*, 1–9.

Polo, S.E., Roche, D., and Almouzni, G. (2006). New histone incorporation marks sites of UV repair in human cells. Cell *127*, 481–493.

Polo, S.E., Theocharis, S.E., Grandin, L., Gambotti, L., Antoni, G., Savignoni, A., Asselain, B., Patsouris, E., and Almouzni, G. (2010). Clinical significance and prognostic value of chromatin assembly factor-1 overexpression in human solid tumours. Histopathology *57*, 716–724.

Prochasson, P., Florens, L., Swanson, S.K., Washburn, M.P., and Workman, J.L. (2005). The HIR corepressor complex binds to nucleosomes generating a distinct protein/DNA complex resistant to remodeling by SWI/SNF. Genes Dev. *19*, 2534–2539.

Rahl, P.B., Lin, C.Y., Seila, A.C., Flynn, R.A., McCuine, S., Burge, C.B., Sharp, P.A., and Young, R.A. (2010). c-Myc regulates transcriptional pause release. Cell *141*, 432–445.

Rai, T.S., Puri, A., McBryan, T., Hoffman, J., Tang, Y., Pchelintsev, N.A., van Tuyn, J., Marmorstein, R., Schultz, D.C., and Adams, P.D. (2011). Human CABIN1 is a functional member of the human HIRA/UBN1/ASF1a histone H3.3 chaperone complex. Mol. Cell. Biol. *31*, 4107–4118.

Ray-Gallet, D., and Almouzni, G. (2010). Nucleosome dynamics and histone variants. Essays Biochem. *48*, 75–87.

Ray-Gallet, D., Quivy, J.P., Scamps, C., Martini, E.M., Lipinski, M., and Almouzni, G. (2002). HIRA is critical for a nucleosome assembly pathway independent of DNA synthesis. Mol. Cell *9*, 1091–1100.

Rugg-Gunn, P.J., Cox, B.J., Ralston, A., and Rossant, J. (2010). Distinct histone modifications in stem cell lines and tissue lineages from the early mouse embryo. Proc. Natl. Acad. Sci. USA *107*, 10783–10790.

Sakai, A., Schwartz, B.E., Goldstein, S., and Ahmad, K. (2009). Transcriptional and developmental functions of the H3.3 histone variant in Drosophila. Curr. Biol. *19*, 1816–1820.

Santenard, A., Ziegler-Birling, C., Koch, M., Tora, L., Bannister, A.J., and Torres-Padilla, M.E. (2010). Heterochromatin formation in the mouse embryo requires critical residues of the histone variant H3.3. Nat. Cell Biol. *12*, 853–862.

Sawatsubashi, S., Murata, T., Lim, J., Fujiki, R., Ito, S., Suzuki, E., Tanabe, M., Zhao, Y., Kimura, S., Fujiyama, S., et al. (2010). A histone chaperone, DEK, transcriptionally coactivates a nuclear receptor. Genes Dev. *24*, 159–170.

Shah, J.V., Botvinick, E., Bonday, Z., Furnari, F., Berns, M., and Cleveland, D.W. (2004). Dynamics of centromere and kinetochore proteins; implications for checkpoint signaling and silencing. Curr. Biol. *14*, 942–952.

Sims, R.J., 3rd, Belotserkovskaya, R., and Reinberg, D. (2004). Elongation by RNA polymerase II: the short and long of it. Genes Dev. *18*, 2437–2468.

Smith, S., and Stillman, B. (1989). Purification and characterization of CAF-I, a human cell factor required for chromatin assembly during DNA replication in vitro. Cell *58*, 15–25.

Stock, J.K., Giadrossi, S., Casanova, M., Brookes, E., Vidal, M., Koseki, H., Brockdorff, N., Fisher, A.G., and Pombo, A. (2007). Ring1-mediated ubiquitination of H2A restrains poised RNA polymerase II at bivalent genes in mouse ES cells. Nat. Cell Biol. *9*, 1428–1435.

Szenker, E., Ray-Gallet, D., and Almouzni, G. (2011). The double face of the histone variant H3.3. Cell Res. *21*, 421–434.

Tagami, H., Ray-Gallet, D., Almouzni, G., and Nakatani, Y. (2004). Histone H3.1 and H3.3 complexes mediate nucleosome assembly pathways dependent or independent of DNA synthesis. Cell *116*, 51–61.

Talbert, P.B., and Henikoff, S. (2010). Histone variants—ancient wrap artists of the epigenome. Nat. Rev. Mol. Cell Biol. *11*, 264–275.

Torres-Padilla, M.E., Bannister, A.J., Hurd, P.J., Kouzarides, T., and Zernicka-Goetz, M. (2006). Dynamic distribution of the replacement histone variant H3.3 in the mouse oocyte and preimplantation embryos. Int. J. Dev. Biol. *50*, 455–461.

van der Heijden, G.W., Dieker, J.W., Derijck, A.A., Muller, S., Berden, J.H., Braat, D.D., van der Vlag, J., and de Boer, P. (2005). Asymmetry in histone H3 variants and lysine methylation between paternal and maternal chromatin of the early mouse zygote. Mech. Dev. *122*, 1008–1022.

von Lindern, M., Fornerod, M., van Baal, S., Jaegle, M., de Wit, T., Buijs, A., and Grosveld, G. (1992). The translocation (6;9), associated with a specific subtype of acute myeloid leukemia, results in the fusion of two genes, dek and can, and the expression of a chimeric, leukemia-specific dek-can mRNA. Mol. Cell. Biol. *12*, 1687–1697.

Wirbelauer, C., Bell, O., and Schübeler, D. (2005). Variant histone H3.3 is deposited at sites of nucleosomal displacement throughout transcribed genes while active histone modifications show a promoter-proximal bias. Genes Dev. *19*, 1761–1766.

Wong, L.H., Ren, H., Williams, E., McGhie, J., Ahn, S., Sim, M., Tam, A., Earle, E., Anderson, M.A., Mann, J., and Choo, K.H. (2009). Histone H3.3 incorporation provides a unique and functionally essential telomeric chromatin in embryonic stem cells. Genome Res. *19*, 404–414.

Wong, L.H., McGhie, J.D., Sim, M., Anderson, M.A., Ahn, S., Hannan, R.D., George, A.J., Morgan, K.A., Mann, J.R., and Choo, K.H. (2010). ATRX interacts with H3.3 in maintaining telomere structural integrity in pluripotent embryonic stem cells. Genome Res. *20*, 351–360.

Wu, R.S., Tsai, S., and Bonner, W.M. (1982). Patterns of histone variant synthesis can distinguish G0 from G1 cells. Cell *31*, 367–374.

Molecular Cell, *Volume 44*

Supplemental Information

Dynamics of Histone H3 Deposition In Vivo Reveal a Targeting Mechanism for H3.3 to Maintain Chromatin Integrity

Dominique Ray-Gallet, Adam Woolfe, Isabelle Vassias, Céline Pellentz, Nicolas Lacoste, Aastha Puri, David C. Schultz, Nikolay A. Pchelintsev, Peter D. Adams, Lars E.T. Jansen, and Geneviève Almouzni

SUPPLEMENTAL EXPERIMENTAL PROCEDURES

siRNA transfection

Small interfering RNAs (siRNA) were purchased from Dharmacon. We used ON-TARGETplus J-013610-07 (HIRA#1), J-013610-06 (HIRA#2), J-014195-05 (UBN1), J-012454-09 (Cabin1), J-004420-05 (DAXX) and D-001810-01 (non-targeting control). SiRNAs p60#1 and p60#2 against CAF-1 p60 and siRNA against ATRX were previously described in (Polo et al., 2006) and (Ritchie et al., 2008), respectively. H3.1-SNAP or H3.3-SNAP cells were transiently transfected using oligofectamine (Invitrogen) for siRNAs.

Cell extracts, immunoprecipitation and Western blotting

For total extracts, cells were lysed directly into Laemmli buffer sample followed by addition of benzonase (Novagen). Cytosolic and nuclear extracts were obtained as previously described (Martini et al., 1998). We prepared chromatin fraction by addition of benzonase to the final pellet followed by sonication.

Immunoprecipitations were carried out overnight at 4°C with the appropriate primary antibody in the presence of 150 mM NaCl and 0.5% NP40 followed by an incubation with Dynabeads protein A, protein G or rat anti-mouse IgM (Invitrogen). For HA immunoprecipitation, we used anti-HA affinity matrix (Roche).

For Western blot analysis, extracts or immunoprecipitated proteins were run on NuPAGE bis-tris 4-12% gels in MOPS buffer (Invitrogen) and transferred to nitrocellulose membrane (Protran). Primary antibodies were detected using horse-radish-peroxidase-conjugated secondary antibodies (Jackson ImmunoResearch Laboratories) and SuperSignal enhanced chemiluminescent detection kit (Pierce). For semi-quantitative analysis of western blot, serial dilutions of protein samples were loaded in order to obtain comparable signals, in the linear range of detection. Chemiluminescent signal was quantified using the ChemiDoc system equipped with a XRS camera and Quantity One software (BioRad).

Antibodies

Antibodies were used at the following dilutions: anti-CAF-1p60 rabbit polyclonal (Green and Almouzni, 2003) western 1:1000 and IF 1:250; anti-CAF-1p150 mouse monoclonal (ab7655, Abcam) 1:500; anti-CAF-1 p48 rabbit polyclonal (ab1765, Abcam) 1:1000; anti-HIRA mouse monoclonal (WC119) (Hall et al., 2001) western and IF 1:100; anti-Cabin1

rabbit polyclonal (ab3349, Abcam) western 1:1000 and IF 1:400; anti-UBN1 mouse monoclonal (ab84953, Abcam) western 1:500 or rabbit polyclonal (Banumathy et al., 2009) western 1:1000 and IF 1:500; anti-γ-tubulin mouse monoclonal (T5326, Sigma) 1:1000; anti-HA epitope rat monoclonal (Roche) 1:1000; anti-H3 rabbit polyclonal (ab1791, Abcam) 1:1000; anti-RNA polymerase II Ser2P mouse monoclonal (clone H5 #MMS-129R, Covance) 1:500; anti-RNA polymerase II Ser5P mouse monoclonal (clone CTD4H8 #05-623, Millipore) 1:1000; anti-Asf1a/b rabbit polyclonal (Mello et al., 2002) 1:1000; anti-DAXX rabbit polyclonal (sc-7152, Santa Cruz); anti-ATRX rabbit polyclonal (sc-15408, Santa Cruz) 1:2000; anti-spt6 rabbit polyclonal (ab32820, Abcam) 1:500; anti-spt16 rabbit polyclonal (sc-28734, Santa Cruz) 1:500; anti-NASP rabbit polyclonal (Cook et al., submitted); anti-DEK rabbit polyclonal (NB100-61058, Novus Biologicals).

Purification of recombinant proteins

For HIRA(His)-UBN1(Flag)-Cabin1(myc) trimeric complex productions, 1 x 10^6 Sf9 cells/ml (of Sf900-III medium) (Invitrogen) were co-infected with viruses for each complex subunit, at an MOI of 1. Infected cells were harvested 48 hours post-infection. To purify protein complexes, cell pellets were lysed by Dounce homogenization in 20 mM Hepes pH 8.0, 500 mM NaCl, supplemented with 5 mM 2-mercaptothanol and protease inhibitors. Clarified supernatants were incubated with anti-flag (M2) agarose (Sigma) for 1 hour. Bound protein(s) were washed with 60 column volumes of lysis buffer prior to elution with 800 μg/ml of flag (M2) peptide (Sigma) for 2 hours at 4°C. Subunit expression and complex composition was confirmed by Western Blot analysis.

Recombinant HIRA(Flag), UBN1(Flag), and Cabin1(Flag) were purified following the method described for the trimeric complex. Recombinant His-Asf1a was expressed in baculovirus infected Sf9 cells. Cell pellets were lysed in 20 mM Hepes pH 8.0, 500 mM NaCl, 10 mM Imidazole, supplemented with 5 mM 2-mercaptothanol and protease inhibitors. The clarified supernatant was incubated with Ni-NTA resin (Qiagen) for 1 hour. The Ni-NTA resin was washed with 60 column volumes of lysis buffer supplemented with 40 mM Imidazole and bound protein was step-eluted with lysis buffer containing 250 mM Imidazole. Peak fractions of His-Asf1a were further purified by size exclusion chromatography (Superdex 75, GE Healthcare) in 20 mM Hepes pH 8.0, 500 mM NaCl, and 5 mM 2-mercaptothanol.

ChIP-seq data analysis

All datasets were downloaded as raw Illumina FASTQ reads from the Short Read Archive (http://www.ncbi.nlm.nih.gov/Traces/sra) and mapped to the mouse genome (NCBI37/mm9 assembly) using the Bowtie aligner (Langmead, 2010) retaining only unique hits with a maximum of 2 mismatches. RNA-seq analysis was used to obtain sets of high, medium and low expressed genes in Mouse ES cells (Guttman et al., 2010) and Human Hela S3 cells (Birney et al., 2007). We utilized RNA-seq data, rather than available microarray data, to obtain precisely the most abundantly expressed isoform for each gene in that cell type. This delineated the start and end of transcripts more precisely, which was important for the H3.3 and Pol II enrichment analysis. Paired end reads were treated as single-end reads and mapped to either the mouse or human genomes respectively (same assemblies) using TopHat (Trapnell et al., 2009) with default settings. Isoform quantification and expression levels was obtained using Cufflinks (Trapnell et al., 2010) using an input

reference set of all known transcripts from the UCSC Known Gene table (Fujita et al., 2011). For each gene, any transcript isoform with an abundance of > 50% was chosen, otherwise the longest isoform was chosen. Any gene with a different gene within 5kb either side were removed from the list of genes, to avoid mixing signals. Transcripts were sorted by FPKM value (Fragments Per Kilobase of exon model per Million mapped fragments) and 800 transcripts each were chosen for high (top 800), medium (800 around the mean FPKM value) and low expressed genes (bottom 800 with FPKM value > 0). Enrichment graphs were carried out using the ShortRead package (Morgan et al., 2009) implemented within the R statistical package. Genome-wide coverage maps were created using the *coverage()* function and, to represent the full nucleosome wrapped sequence, reads were extended to a length of 150bp in the direction of the read. Read coverage was normalized by the total number of mapped reads. To correct for any underling biases due to mappability, MNase digestion bias or the aneuploidy nature of the Hela cell line, we further normalized all mean IP signals by the mean input signal at each window across all genes.

Transcription factor binding site peaks were created for each factor from Bowtie mapping output using the FindPeaks4 program (v4.0.13) (Fejes et al., 2008). Reads were extended to a length of 150bp and peaks were created setting the subpeak parameter to 0.4 (peaks are split if there is a subpeak that falls 40% below the maximum peak), the trimming parameter to 0.2 (peaks are trimmed once they fall below 20% of the maximum peak height) and a p-value threshold of $P<1e^{-4}$. The GFP input dataset was used as a background control. Peaks were filtered out if located within 2.5kb of a known mouse transcript (downloaded from the RefSeq, Ensembl or Known genes tables from the UCSC genome browser), a set of novel lncRNAs identified in mESCs (Guttman et al., 2009) or within 2kb of another peak from the same factor (to avoid mixing signals). Peaks were further filtered for the presence of H3K4me3 (to avoid any peaks located in novel promoter regions) by removing any peak covered by more than an average of 1 aligned read from the H3K4me3 ChIP-seq dataset. In addition to a lack of H3K4me3, we found all sites were enriched for H3K4me1 and H3K27ac and had no enrichment for H3K27me3 (Figure S5), suggesting the sites were active regulatory elements in mESCs. We used the top 1000 remaining peaks (sorted by p-value) for each factor to allow for fair comparison between factors. To measure HIRA-dependent H3.3 deposition within a set of binding sites for a specific factor, we used a measure ΔH3.3, calculated by dividing the mean H3.3 coverage in binding sites in HIRA deficient cells by mean H3.3 coverage in binding sites in wild-type cells. ΔH3.3 values close to 1 represent little or no change in H3.3 coverage in HIRA deficient cells compared to WT, while those less than 1 represent an overall decrease and those above 1, an overall increase in mean H3.3 coverage. Mean coverage for a set of binding sites (carried out for H3.3 and Pol II) was measured as the sum of the number of extended reads per base per million mapped reads divided by the total number of bases in all binding sites.

Figure S1

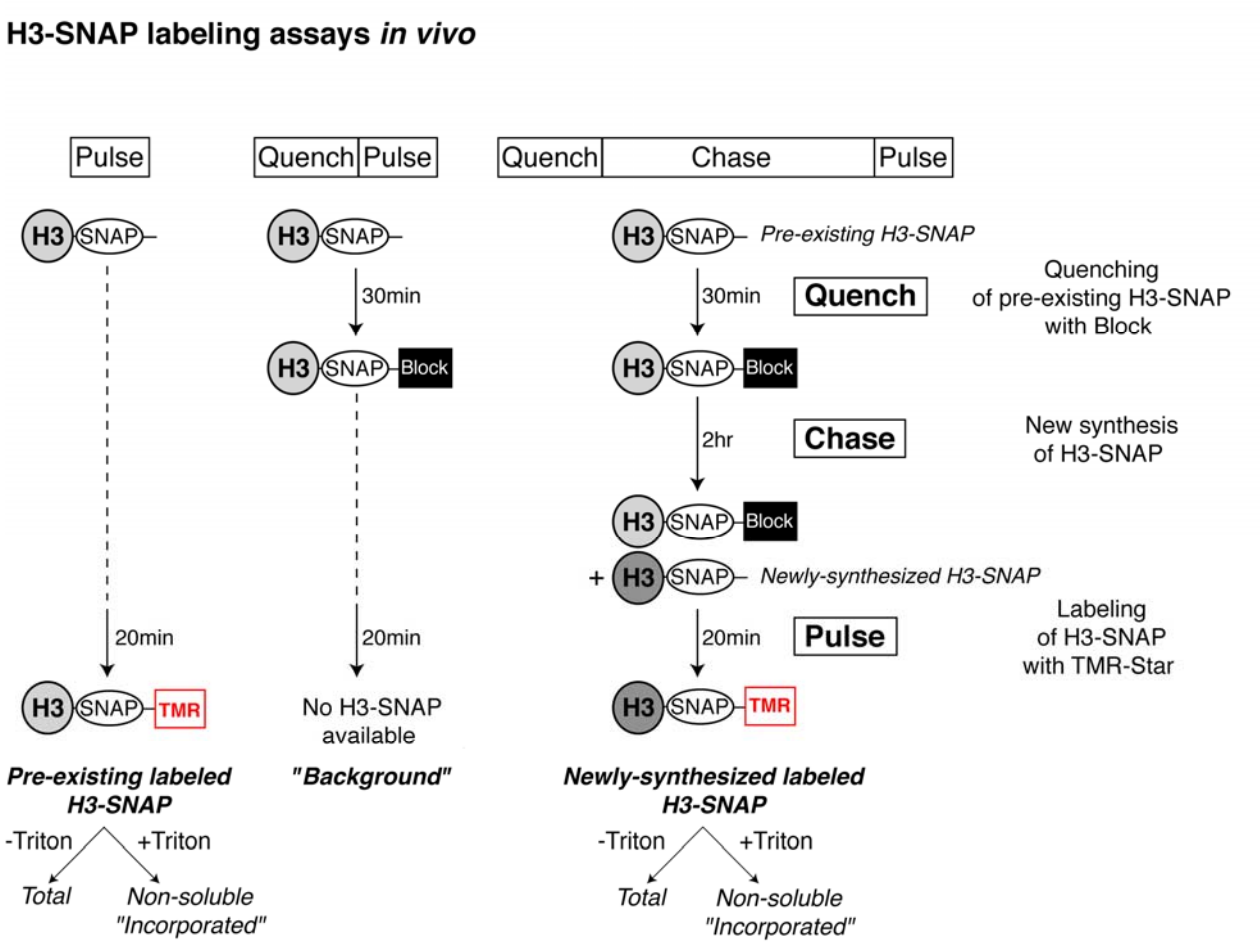

Figure S1. Related to Figure 1

Scheme of the assays for labeling H3-SNAP histones in Pulse, Quench-Pulse and Quench-Chase-Pulse experiments *in vivo*. The Pulse labels pre-existing H3-SNAP with red fluorescent TMR-Star, the Quench-Pulse quenches pre-existing H3-SNAP with non-fluorescent Block preventing their subsequent labeling with TMR-Star and the "Quench-Chase-Pulse" labels new H3-SNAP synthesized during the 2 hr-chase. Either total (-triton) or incorporated (non-soluble) (+triton) H3-SNAP are analyzed.

Figure S2

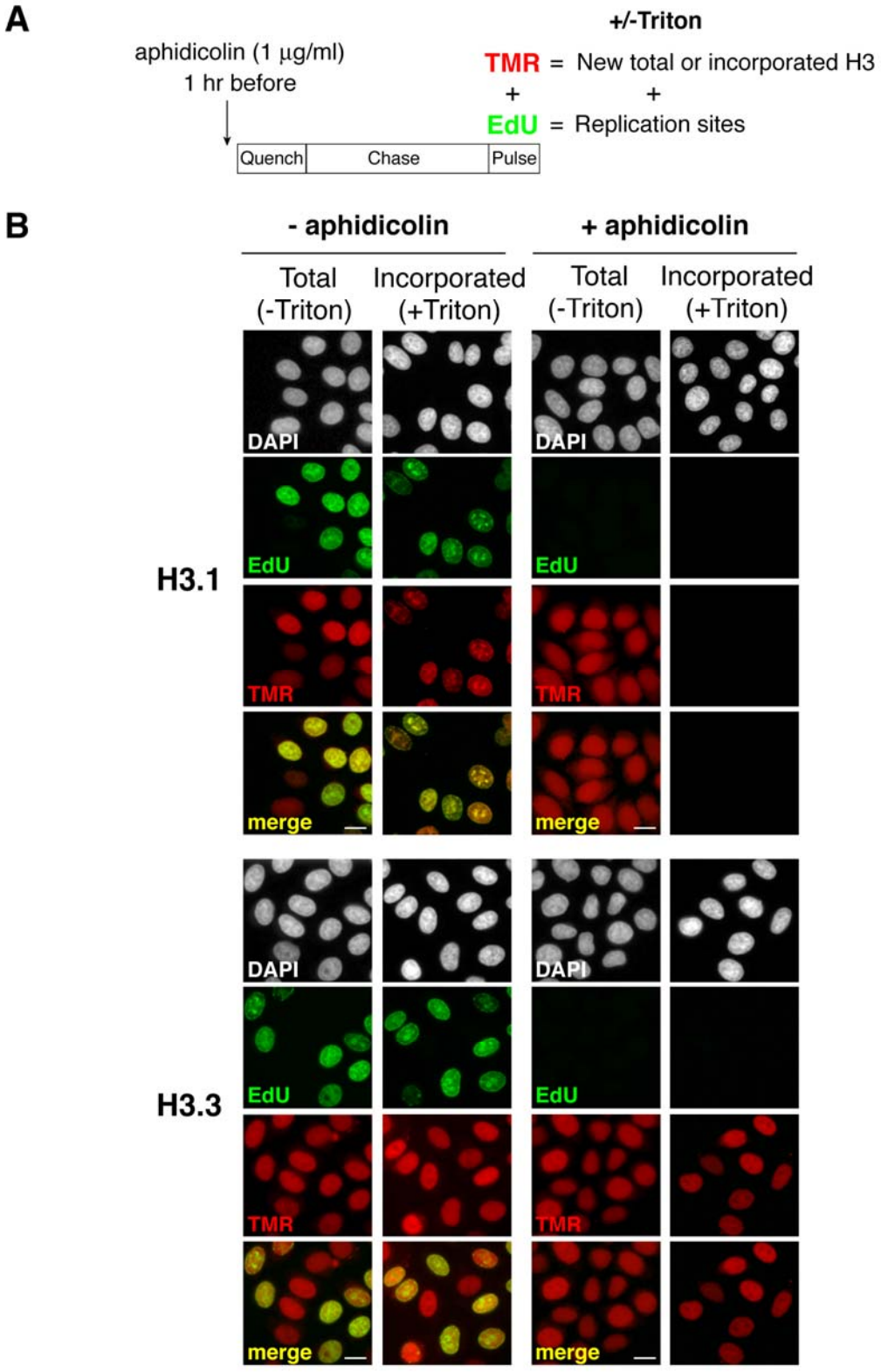
A
+/-Triton
aphidicolin (1 μg/ml)
1 hr before
TMR = New total or incorporated H3
+ +
EdU = Replication sites
Quench
Chase
Pulse
B
- aphidicolin
+ aphidicolin
Total (-Triton)
Incorporated (+Triton)
Total (-Triton)
Incorporated (+Triton)
H3.1
H3.3
DAPI
EdU
TMR
merge

Figure S2. Related to Figure 2

(A) *In vivo* labeling scheme of newly-synthesized H3-SNAP by the Quench-Chase-Pulse experiment and of replication sites with EdU during the Pulse coupled or not with aphidicolin treatment to block replication. The cells are treated or not with triton before fixation to visualize incorporated or total H3-SNAP, respectively.

(B) Fluorescent microscopy visualization of replication sites (EdU, green) and total or incorporated newly-synthesized H3.1- and H3.3-SNAP (red) after *in vivo* labeling in presence or not of aphidicolin. Scale bar, 10 μm.

Figure S3

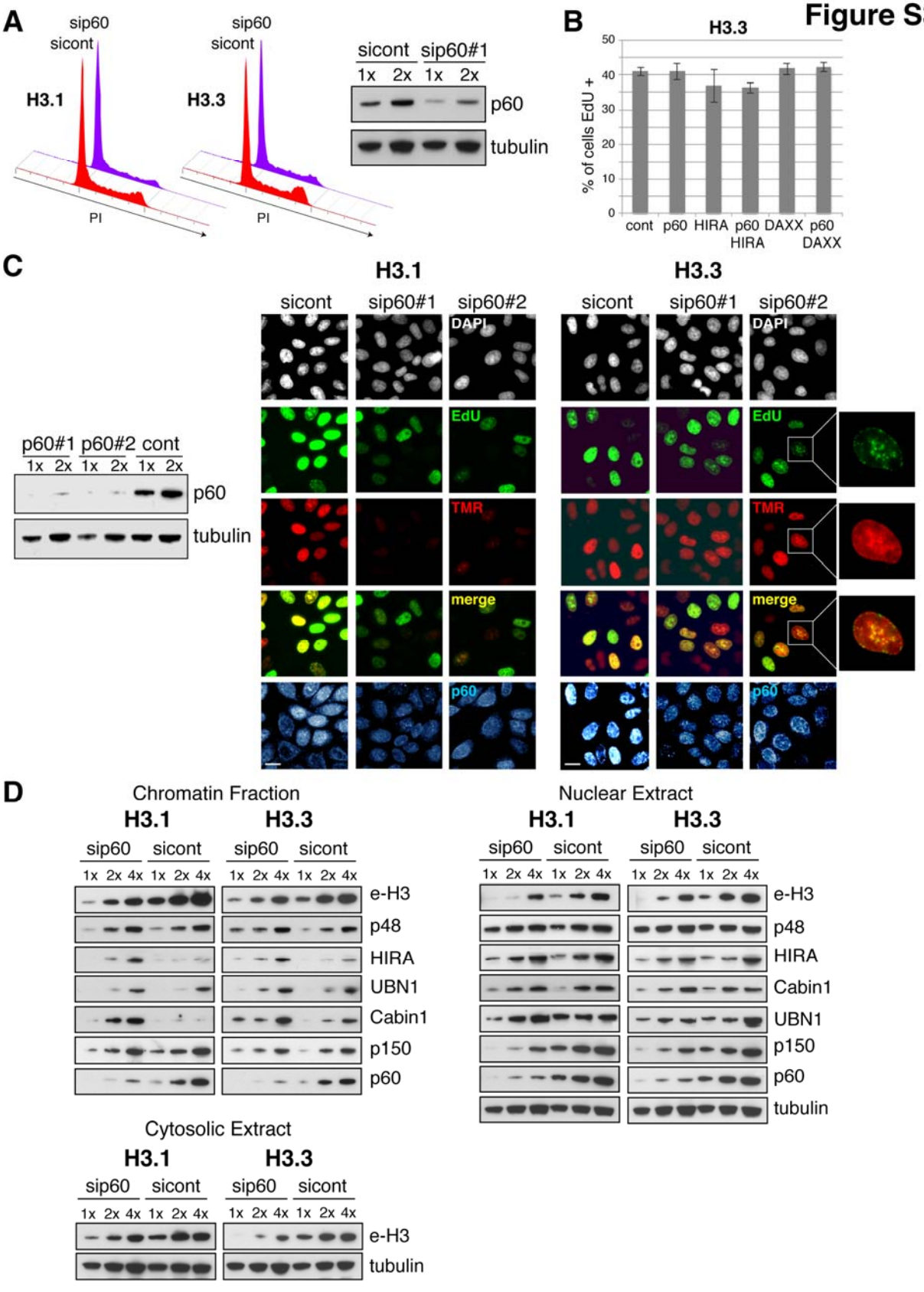
A
sip60
sicont
H3.1
H3.3
PI
sicont sip60#1
1x 2x 1x 2x
p60
tubulin
B
H3.3
% of cells EdU +
cont p60 HIRA p60 HIRA DAXX p60 DAXX
C
H3.1
H3.3
sicont sip60#1 sip60#2
DAPI
EdU
TMR
merge
p60
p60#1 p60#2 cont
1x 2x 1x 2x 1x 2x
p60
tubulin
D
Chromatin Fraction
Nuclear Extract
Cytosolic Extract
H3.1 H3.3
sip60 sicont
1x 2x 4x
e-H3
p48
HIRA
UBN1
Cabin1
p150
p60
tubulin

Figure S3. Related to Figure 3

(A) Cell cycle profiles of HeLa H3.1 and HeLa H3.3 cells treated for 48 hr with siRNA against CAF-1 p60 or control. PI; Propidium Iodide. The efficiency of siRNA treatments shown in figure 3B is assessed by Western blotting of total extracts of H3.1 cells (-triton) treated with siRNAs against CAF-1 p60 (sip60#1) or control (sicont).

(B) Quantification of the percentage of cells that are EdU positive after the indicated siRNA treatments for 48 hr. Error bars indicate standard deviation in at least three experiments.

(C) (Left) Assessment of the efficiency of 48 hr siRNAs treatment against p60 by Western blotting of total extracts. (Right) Fluorescent microscopy visualization of replication sites (EdU, green) and new incorporated H3.1 or H3.3 (red) after siRNAs transfection against CAF-1 p60#1, CAF-1 p60#2 or control. CAF-1 p60 is detected by immunofluorescence (blue). The insets represent enlarged images of one selected cell. Scale bar, 10 μm.

(D) Western blot analysis of the chromatin, nuclear and cytosolic fractions prepared from H3.1 or H3.3 cells treated for 48 hr with siRNA against CAF-1 p60 or control. The H3.1 and H3.3 decrease in the chromatin fractions by about 6-fold and 2-fold respectively supported the stronger impact of p60 depletion on new H3.1 incorporation (see Figure 3B). The presence of tagged histones in lower amounts in nuclear an cytosolic extracts from sip60-treated cells suggests that depletion of CAF-1 may also have a general effect on histone synthesis and/or stability.

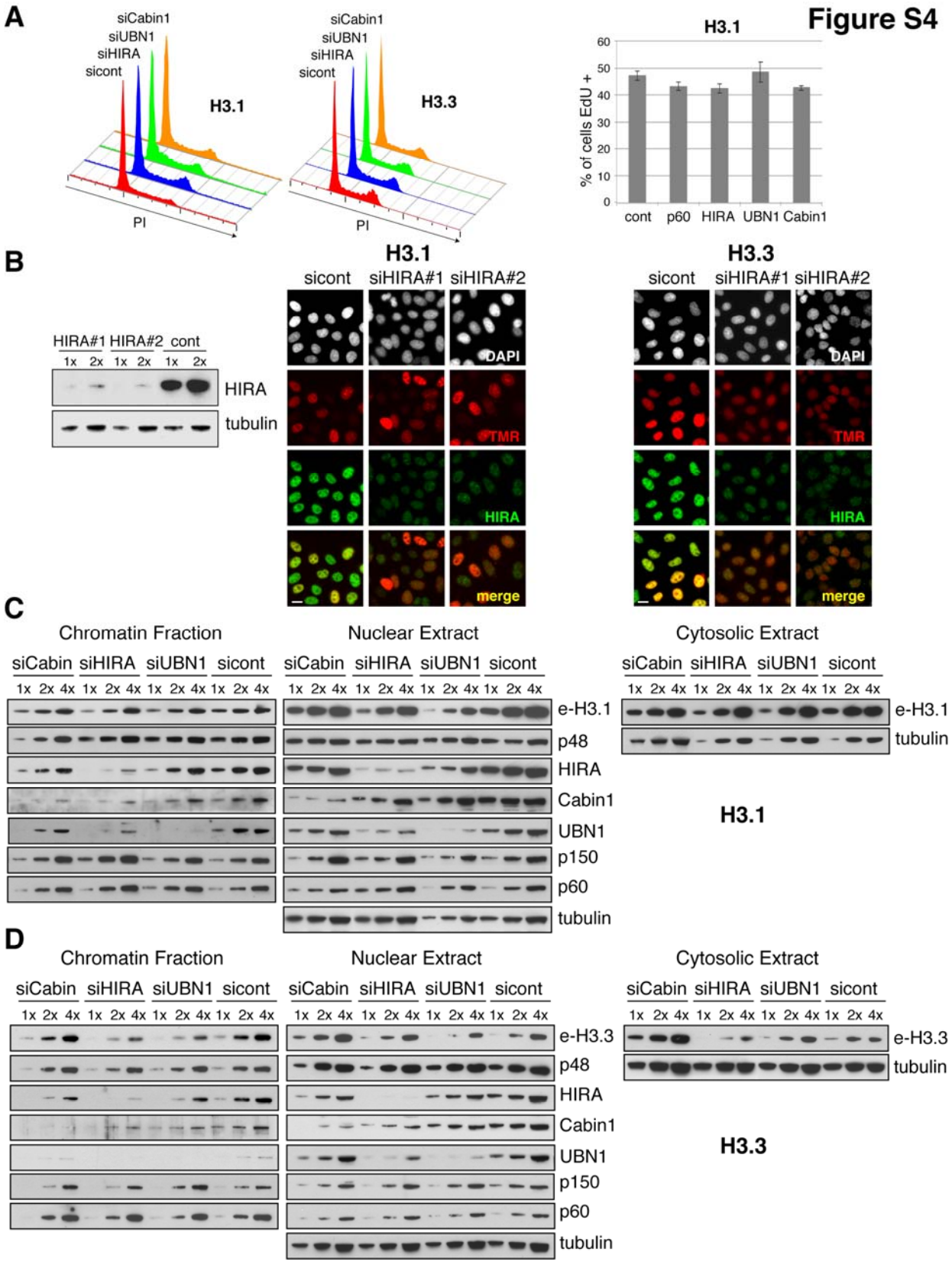
Figure S4
A
siCabin1
siUBN1
siHIRA
sicont
H3.1
H3.3
PI
% of cells EdU +
cont
p60
HIRA
UBN1
Cabin1
B
HIRA#1
HIRA#2
cont
1x
2x
HIRA
tubulin
sicont
siHIRA#1
siHIRA#2
DAPI
TMR
HIRA
merge
C
Chromatin Fraction
Nuclear Extract
Cytosolic Extract
siCabin
siHIRA
siUBN1
sicont
1x 2x 4x
e-H3.1
p48
HIRA
Cabin1
UBN1
p150
p60
tubulin
H3.1
D
e-H3.3
H3.3

Figure S4. Related to Figure 4

(A) (Left) Cell cycle profiles of HeLa H3.1 and H3.3 cells treated for 72 hr with siRNA against HIRA, UBN1, Cabin1 or control. PI; Propidium Iodide. (Right) Quantification of the percentage of cells that are EdU positive after the indicated siRNA treatments for 72 hr. Error bars indicate standard deviation in at least three experiments.

(B) (Left) Assessment of the efficiency of 72 hr siRNAs treatment against HIRA by Western blotting of total extracts. (Right) Fluorescent microscopy visualization of new incorporated H3.1 or H3.3 (red) after siRNAs transfection against HIRA#1, HIRA#2 or control. HIRA is detected by immunofluorescence (green). Scale bar, 10 μm.

(C) and (D) Western blot analysis of chromatin, nuclear and cytosolic fractions prepared from H3.1 and H3.3 cells respectively treated for 72 hr with siRNA against Cabin1, HIRA, UBN1 or control. Chromatin fractions showed that in siCabin1-, siHIRA- or siUBN1-treated cells the amount of H3.1 did not change while H3.3 decreased by about 3-fold in both siHIRA- and siUBN1- but not in siCabin1-transfected cells. This supported the stronger impact of HIRA complex and UBN1 depletions on new H3.3 incorporation (see Figure 4C-D). Interestingly, we detected an increase of H3.3 but not of H3.1 in the nuclear and cytosolic extracts of siCabin1-treated cells suggesting that although Cabin1 is not a major player in the deposition per se of H3.3, it may contribute to regulating its metabolism.

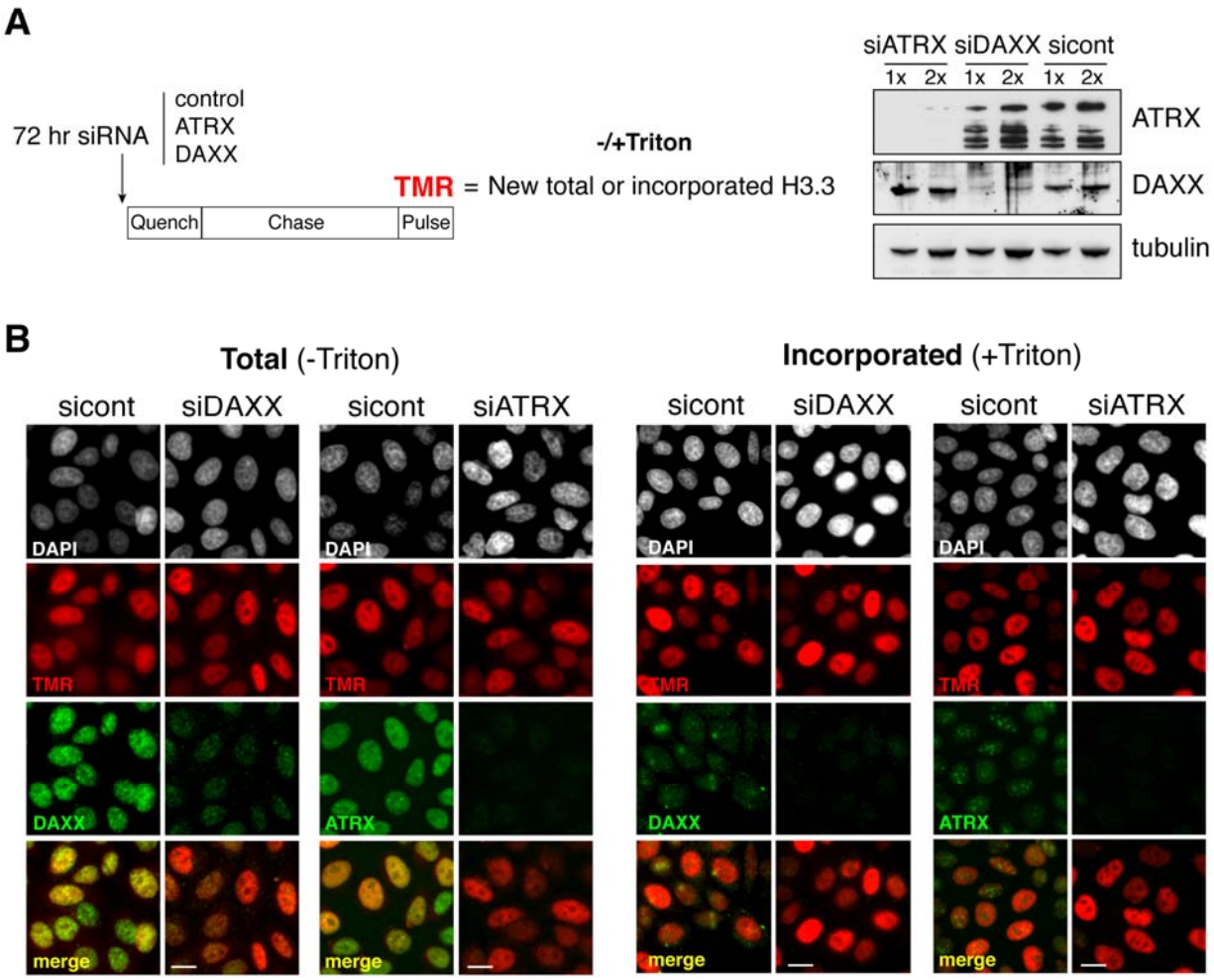

Figure S5. Related to Figure 4

(A) (Left) *In vivo* labeling scheme of newly-synthesized H3.3-SNAP by the Quench-Chase-Pulse experiment coupled with transfection of siRNAs against DAXX or ATRX 72hr before the *in vivo* labeling. The cells are treated or not with triton before fixation to visualize incorporated or total H3-SNAP, respectively. (Right) Assessment of the siRNAs efficiency by Western blotting of total extracts from cells treated with the indicated siRNAs.

(B) Fluorescent microscopy visualization of total or incorporated newly-synthesized H3.3-SNAP (red) after *in vivo* labeling. DAXX and ATRX are detected by immunofluorescence (green). Scale bar, 10 µm.

Figure S6

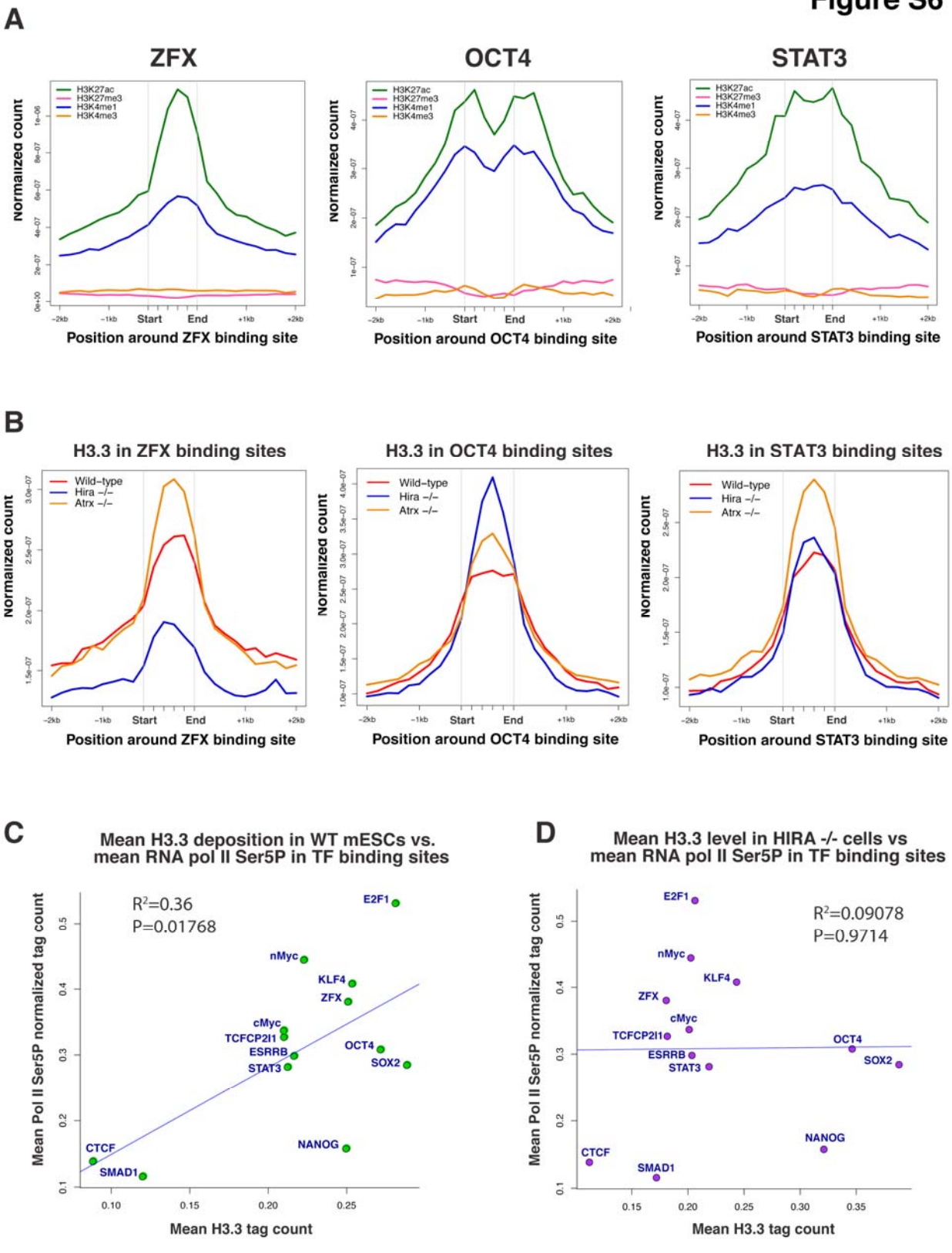
A
ZFX
OCT4
STAT3
H3K27ac
H3K27me3
H3K4me1
H3K4me3
Normalized count
Start
End
Position around ZFX binding site
Position around OCT4 binding site
Position around STAT3 binding site
B
H3.3 in ZFX binding sites
H3.3 in OCT4 binding sites
H3.3 in STAT3 binding sites
Wild-type
Hira −/−
Atrx −/−
C
Mean H3.3 deposition in WT mESCs vs.
mean RNA pol II Ser5P in TF binding sites
R²=0.36
P=0.01768
Mean Pol II Ser5P normalized tag count
Mean H3.3 tag count
E2F1
nMyc
KLF4
ZFX
cMyc
TCFCP2l1
ESRRB
STAT3
OCT4
SOX2
NANOG
CTCF
SMAD1
D
Mean H3.3 level in HIRA -/- cells vs
mean RNA pol II Ser5P in TF binding sites
R²=0.09078
P=0.9714

Figure S6. Related to Figure 5

(A) Histone modification patterns in and around three example sets of intergenic TFBS peaks (ZFX, OCT4 and STAT3) used in this study. All binding sites have low levels of H3K4me3 indicating they are unlikely to be part of promoters and low levels of H3K27me3, indicating they are not repressed. Binding sites are also enriched for H3K4me1 and H3K27ac, histone marks associated with active enhancers, although the pattern of enrichment in and around the binding site (delineated by two grey lines) differs significantly between factors. Profiles were created by summing read coverage per mapped read in 200bp sliding windows outside of the binding site and normalizing by the length of the window and the number of binding sites. Inside binding sites, the binding site was divided into 5 bins of equal length, and read coverage per mapped read was summed for each bin over all binding sites and then normalized by the total number of bases in each bin.

(B) H3.3 levels in wild-type, HIRA-deficient and ATRX-deficient mESCs in and around three example sets of TFBS peaks (ZFX, OCT4 and STAT3) used in this study. All binding sites show distinct enrichment directly within the binding site (delineated by two grey lines). For some factors, H3.3 level in the binding site was reduced in HIRA deficient cells compared to wild-type cells (e.g. ZFX). For other factors, the level of H3.3 was higher in HIRA deficient cells than wild-type cells (e.g. OCT4) or remained virtually the same (e.g. STAT3). Note these are averaged profiles and therefore show only general trends, rather than what is true for each binding site in the set. There is a proportion of binding sites that are lower or higher in HIRA deficient cells in each case, but the proportion of these is different in each factor. Graphs were produced as described in (A).

(C) A correlative analysis of mean H3.3 levels in wild-type mESCs in sets of 13 TFBS peaks and mean Pol II Ser5P in the same binding sites. A weak but significant correlation was found between H3.3 and Pol II levels, suggesting that Pol II influences H3.3 deposition in some TFBSs.

(D) The same correlative analysis between mean H3.3 levels in HIRA deficient mESCs in TFBSs and mean Pol II Ser5P. The weak correlation seen for wild-type mESCs has now been completely abrogated, confirming that Pol II influences HIRA-dependent H3.3 deposition but not HIRA-independent H3.3 deposition.

SUPPLEMENTAL REFERENCES

Banumathy, G., Somaiah, N., Zhang, R., Tang, Y., Hoffmann, J., Andrake, M., Ceulemans, H., Schultz, D., Marmorstein, R., and Adams, P.D. (2009). Human UBN1 is an ortholog of yeast Hpc2p and has an essential role in the HIRA/ASF1a chromatin-remodeling pathway in senescent cells. Mol Cell Biol *29*, 758-770.

Birney, E., Stamatoyannopoulos, J.A., Dutta, A., Guigo, R., Gingeras, T.R., Margulies, E.H., Weng, Z., Snyder, M., Dermitzakis, E.T., Thurman, R.E.*, et al.* (2007). Identification and analysis of functional elements in 1% of the human genome by the ENCODE pilot project. Nature *447*, 799-816.

Fejes, A.P., Robertson, G., Bilenky, M., Varhol, R., Bainbridge, M., and Jones, S.J. (2008). FindPeaks 3.1: a tool for identifying areas of enrichment from massively parallel short-read sequencing technology. Bioinformatics *24*, 1729-1730.

Fujita, P.A., Rhead, B., Zweig, A.S., Hinrichs, A.S., Karolchik, D., Cline, M.S., Goldman, M., Barber, G.P., Clawson, H., Coelho, A.*, et al.* (2011). The UCSC Genome Browser database: update 2011. Nucleic Acids Res *39*, D876-882.

Green, C.M., and Almouzni, G. (2003). Local action of the chromatin assembly factor CAF-1 at sites of nucleotide excision repair in vivo. EMBO J *22*, 5163-5174.

Guttman, M., Amit, I., Garber, M., French, C., Lin, M.F., Feldser, D., Huarte, M., Zuk, O., Carey, B.W., Cassady, J.P.*, et al.* (2009). Chromatin signature reveals over a thousand highly conserved large non-coding RNAs in mammals. Nature *458*, 223-227.

Guttman, M., Garber, M., Levin, J.Z., Donaghey, J., Robinson, J., Adiconis, X., Fan, L., Koziol, M.J., Gnirke, A., Nusbaum, C.*, et al.* (2010). Ab initio reconstruction of cell type-specific transcriptomes in mouse reveals the conserved multi-exonic structure of lincRNAs. Nat Biotechnol *28*, 503-510.

Hall, C., Nelson, D.M., Ye, X., Baker, K., DeCaprio, J.A., Seeholzer, S., Lipinski, M., and Adams, P.D. (2001). HIRA, the human homologue of yeast Hir1p and Hir2p, is a novel cyclin- cdk2 substrate whose expression blocks S-phase progression. Mol Cell Biol *21*, 1854-1865.

Langmead, B. (2010). Aligning short sequencing reads with Bowtie. Curr Protoc Bioinformatics *Chapter 11*, Unit 11 17.

Martini, E., Roche, D.M., Marheineke, K., Verreault, A., and Almouzni, G. (1998). Recruitment of phosphorylated chromatin assembly factor 1 to chromatin after UV irradiation of human cells. J Cell Biol *143*, 563-575.

Mello, J.A., Sillje, H.H., Roche, D.M., Kirschner, D.B., Nigg, E.A., and Almouzni, G. (2002). Human Asf1 and CAF-1 interact and synergize in a repair-coupled nucleosome assembly pathway. EMBO Rep *3*, 329-334.

Morgan, M., Anders, S., Lawrence, M., Aboyoun, P., Pages, H., and Gentleman, R. (2009). ShortRead: a bioconductor package for input, quality assessment and exploration of high-throughput sequence data. Bioinformatics *25*, 2607-2608.

Polo, S.E., Roche, D., and Almouzni, G. (2006). New histone incorporation marks sites of UV repair in human cells. Cell *127*, 481-493.

Ritchie, K., Seah, C., Moulin, J., Isaac, C., Dick, F., and Berube, N.G. (2008). Loss of ATRX leads to chromosome cohesion and congression defects. J Cell Biol *180*, 315-324.

Trapnell, C., Pachter, L., and Salzberg, S.L. (2009). TopHat: discovering splice junctions with RNA-Seq. Bioinformatics *25*, 1105-1111.

Trapnell, C., Williams, B.A., Pertea, G., Mortazavi, A., Kwan, G., van Baren, M.J., Salzberg, S.L., Wold, B.J., and Pachter, L. (2010). Transcript assembly and quantification by RNA-Seq reveals unannotated transcripts and isoform switching during cell differentiation. Nat Biotechnol *28*, 511-515.